Two cowpea Rubisco activase isoforms for crop thermotolerance

Armida Gjindali; Rhiannon Page; Catherine J. Ashton; Ingrid Robertson; Mike T. Page; Duncan Bloemers; Peter D. Gould; Dawn Worrall; Douglas J. Orr; Elizabete Carmo-Silva
Lancaster Environment Centre, Lancaster University, Lancaster, LA1 4YQ, UK
Corresponding author email: e.carmosilva@lancaster.ac.uk

Submission date: 31st January 2025
Number of figures: 4 (all figures in colour)
Number of tables: 2
Number of Supporting Information figures: 15 (all figures in colour)
Number of Supporting Information tables: 10
Word count: 9833

Summary

- A vital crop for sub-Saharan Africa, cowpea productivity is threatened by climate change, including increased heatwave intensity, duration, and frequency. Rubisco activase (Rca) is a key molecular chaperone that maintains Rubisco activity and due to its thermal sensitivity is a key target for improving crop climate resilience.
- We identified and characterised four Rca isoforms in *Vigna unguiculata* (L.) Walp. cv. IT97K-499-35 *in vitro*: Rca1β, Rca8α, Rca10α and Rca10β. Cowpea leaf and plant growth traits were also investigated during a 5-day +10 °C heatwave that included assessment of Rubisco and Rca activity in leaf extracts, and relative changes in the abundance of the four Rca isoforms.
- Cowpea Rca10α and Rca10β had higher thermal maxima, broader thermal optima and higher rates of ATP hydrolysis and Rubisco reactivation *in vitro*. In the absence of water deficit, the heatwave caused only mild effects, including increases in leaf temperature and expression of *Rca10*, small decreases in Rubisco activity and activation state, and unaltered temperature response of Rubisco activation by Rca.
- The superior Rca10α and Rca10β isoforms offer the prospect of enhancing the thermotolerance of cowpea and other crops in anticipation of more extreme future heatwaves.

Keywords: Activase, cowpea, heat stress, photosynthesis, Rca, Rubisco, temperature response, *Vigna unguiculata*.

Introduction

Changes in global temperatures including heatwave events pose significant threats to global food security (Moore *et al.*, 2021), making increased crop resilience against heat stress imperative (Song *et al.*, 2023). Regions closer to the equator, particularly sub-Saharan Africa, are the most vulnerable to rising temperatures (Harboure, 2024). Elevated temperatures can lead to decreased photosynthesis and plant growth (Hatfield & Prueger, 2011; Bagati *et al.*, 2021; Zahra *et al.*, 2023; Becker *et al.*, 2023). Cowpea (*Vigna unguiculata* (L.) Walp) is a major source of protein for populations in sub-Saharan Africa and, despite being adapted to a warm climate, it is still vulnerable to heat stress – even a 1 °C increase in night temperature can result in significant yield loss (Warrag & Hall, 1984; Gonçalves *et al.*, 2016; Mohammed *et al.*, 2024). Therefore, it is imperative to identify physiological and biochemical traits that confer thermotolerance in cowpea to develop heat resilient crops (Barros *et al.*, 2021).

Moderate heat stress, defined as temperatures up to 40 °C (Crafts-Brandner & Salvucci, 2000; Kumar *et al.*, 2009; Ara *et al.*, 2013), has a profound impact on plant photosynthesis, adversely affecting both the electron transport chain and the Calvin-Benson-Bassham (CBB) cycle (Chen *et al.*, 2022). Rubisco and chlorophyll leaf content also decline under moderate heat stress (Mathur *et al.*, 2014). Chlorophyll biosynthesis enzymes exhibit susceptibility to heat stress; however, the reduction in Rubisco content cannot be attributed to denaturation of Rubisco, as alterations in secondary structure are observed only at temperatures exceeding 45 °C (Li *et al.*, 2002; Mathur *et al.*, 2014). Increased temperatures enhance Rubisco carboxylation activity; but also lead to reduced Rubisco specificity and increased O_2 diffusion, both of which result in higher oxygenation over carboxylation and increased photorespiration (Hermida-Carrera *et al.*, 2016; Galmés *et al.*, 2016). Importantly, photorespiration does not fully account for the decline in carbon assimilation during moderate heat stress, as the Rubisco activation state has been demonstrated to decrease under both photorespiratory and non-photorespiratory conditions during mild heat stress (Feller *et al.*, 1998; Crafts-Brandner & Law, 2000; Galmés *et al.*, 2016).

Numerous studies have demonstrated that Rubisco inactivation is one of the primary causes of reduced photosynthetic efficiency during moderate heat stress (Feller *et al.*, 1998; Crafts-Brandner & Law, 2000; Portis, 2003; Ristic *et al.*, 2009; Carmo-Silva *et al.*, 2015; Perdomo *et al.*, 2017; Wijewardene *et al.*, 2021; Scafaro *et al.*, 2023). To catalyse carboxylation or oxygenation, Rubisco catalytic sites require binding of CO_2 and Mg^{2+} as cofactors to form the active carbamylated Rubisco prior to binding the substrate ribulose 1,5-biphosphate (RuBP). Rubisco can become inactivated by the binding of inhibitory sugar phosphates to carbamylated catalytic sites or by misfire products that cannot dissociate and maintain

catalytic sites in their closed, inactive conformation (Orr *et al.*, 2023). Inactivation can also occur when RuBP binds to an uncarbamylated Rubisco catalytic site. Inhibited Rubisco requires its molecular chaperone Rubisco activase (Rca) to restore its activity (Carmo-Silva & Salvucci, 2013). Rca is a nuclear encoded protein that belongs to the AAA+ ATPases superfamily (Hazra *et al.*, 2015) and, in its active multimeric form, exhibits two activities: ATP hydrolysis and Rubisco reactivation (Bhat *et al.*, 2017; Serban *et al.*, 2018). Rca docks on Rubisco's large subunit and, using ATP, performs conformational remodelling to release the inhibitory compound, thus modulating Rubisco activity by facilitating the dissociation of bound inhibitors. Elevated temperatures increase the frequency of Rubisco inactivation due to higher concentrations of some inhibitory substrates (Salvucci & Crafts-Brandner, 2004, p. 20). Furthermore, although Rubisco is a relatively thermostable enzyme, Rca is thermolabile and even a moderate increase in temperature results in loss of its activity (Crafts-Brandner & Salvucci, 2000; Salvucci *et al.*, 2001).

Rca isoforms within a single species vary in their regulatory properties (Zhang & Portis, 1999; Carmo-Silva & Salvucci, 2013; Perdomo *et al.*, 2019; Scafaro *et al.*, 2019b). Many species express two types of Rca isoforms: longer α isoforms (43-47 kDa) and shorter β isoforms (41-43 kDa) that can be encoded either by individual genes or the same gene via alternative splicing (Carmo-Silva *et al.*, 2015). Rca α isoforms contain a C-terminal extension with two cysteine residues shown to form a disulfide bond which is regulated by thioredoxin-f in *Arabidopsis* (Zhang & Portis, 1999). This regulatory mechanism links Rubisco activity with alterations in the redox potential induced by environmental stimuli, such as high light (Zhang *et al.*, 2002; Perdomo *et al.*, 2021). The redox regulation is species-specific, with Solanaceae species such as tobacco (*Nicotiana tabacum* L.) and tomato (*Solanum lycopersicum* L.) containing only the β Rca isoform that lacks the cysteine residues and the redox regulation of the enzyme (Carmo-Silva & Salvucci, 2013). In species containing only redox insensitive Rca, light regulation appears to be mediated by changes in the ADP/ATP ratio of the chloroplast (Carmo-Silva & Salvucci, 2013).

In addition to variation in the number of genes and the isoforms they produce, the expression and relative abundance of Rca isoforms vary among species and as a response to temperature (Law & Crafts-Brandner, 2001; Wang *et al.*, 2010; Degen *et al.*, 2020; Perdomo *et al.*, 2021). In rice (*Oryza sativa* L.) two Rca isoforms are produced via alternative splicing and while Rca β is more abundant under optimal steady state conditions (Wang *et al.*, 2010), heat stress induces upregulation of Rca α (Scafaro *et al.*, 2016). In maize (*Zea mays* L.) the two isoforms derive from two genes *ZmRcaα* and *ZmRcaβ* encoding an α (43 kDa) and a β (41 kDa) isoform respectively (Yin *et al.*, 2014). Under optimal temperature conditions, the ZmRca β protein isoform is expressed in higher levels

108 than ZmRca α and both exhibit comparable diurnal variation in expression levels (Ristic *et*
109 *al.*, 2009). Jiménez *et al*. reported an increase in ZmRca α in seedlings exposed to higher
110 temperatures, however in more mature heat-treated plants this effect was not consistent
111 (Ristic *et al.*, 2009; Stainbrook *et al.*, 2024). In wheat (*Triticum aestivum* L.) there are two
112 *Rca* genes, one of which produces a β isoform while the other (*TaRca2*) is alternatively
113 spliced and produces both an α and a β isoform (Nagarajan & Gill, 2018). The Rca α/β ratio
114 changes when wheat is exposed to heat stress, suggesting that the relative abundance of
115 the different Rca isoforms is linked with the physiological response to heat stress (Warrag &
116 Hall, 1984; Crafts-Brandner & Salvucci, 2000). By contrast, in *Arabidopsis* the Rca isoform
117 ratio is not impacted by heat, with the α and β isoforms originating from alternative splicing
118 continuing to be expressed at a 1:1 ratio (Zhang & Portis, 1999). These species-specific
119 responses of Rca and Rubisco regulation to heat stress illustrate the need to investigate this
120 system directly in the crop of interest.

121 While the exact mechanism of Rca deactivation at high temperatures is still not fully
122 understood, it is evident that the optimum temperature range for Rca is species-specific and
123 in tune with the photosynthetic optimum (Scafaro *et al.*, 2016). Therefore, the temperature at
124 which Rca loses its activity depends on environmental acclimation; i.e., plants that grow at
125 high temperatures, such as cotton and agave, maintain Rca activity at higher temperatures
126 (Salvucci & Crafts-Brandner, 2004; Carmo-Silva & Salvucci, 2011; Scafaro *et al.*, 2016;
127 Shivhare & Mueller-Cajar, 2017). Rca thermotolerance also differs between closely related
128 species and among the native Rca isoforms within a plant species. The wild rice species
129 *Oryza australiensis* Domin and *Oryza meridionalis* Ng. contain thermostable Rca isoforms
130 that enable sustained high Rubisco activity and photosynthetic rate even at 45 °C (Scafaro
131 *et al.*, 2016, 2018). In rice, spinach and cotton, the α isoform exhibits higher thermostability
132 whereas in wheat, it is one of the two shorter β (TaRca1β) isoforms that is most
133 thermostable (Kurek *et al.*, 2007; Wang *et al.*, 2010; Keown & Pearce, 2014; Degen *et al.*,
134 2020). Increasing the thermostability of Rca is considered one of the most promising
135 strategies for increasing Rubisco activity and enhancing photosynthesis under elevated
136 temperature (Carmo-Silva *et al.*, 2015; Wijewardene *et al.*, 2021).

137 In this study we identified four Rca isoforms in cowpea encoded by three genes: *Rca1*, *Rca8*
138 and *Rca10*, with the latter producing two isoforms via alternative splicing. Characterisation of
139 their ATPase and Rubisco reactivation activities across a range of temperatures *in vitro*
140 revealed that the two Rca10 protein isoforms have higher thermal maxima and broader
141 thermal optima for both activities. We then examined the effect of moderate heat stress
142 during a 5-day heatwave at 38 °C (+10°C compared to control) on the expression and
143 abundance of Rca isoforms and subsequent impacts on Rubisco activation in the leaves of

young cowpea plants. Heat treatment resulted in decreased Rubisco activation state and upregulation of *Rca8a* and *Rca10*, however *Rca10* levels were consistently the lowest. Despite upregulation of the more thermotolerant isoforms, the temperature profile of Rubisco reactivation by Rca in leaf extracts remained unaltered in heat-treated plants. Leaf temperature increased by 6 °C during the heatwave, reaching 32 °C, which is within the temperature range where Rca activity is maintained above 70% of the maximum (T_{opt}) for all isoforms. We therefore conclude that warm-adapted cowpea plants can cope with the mild heat stress induced by a 5-day heatwave at 38 °C in the absence of water deficit, which did not impair Rca function. Overexpression of the most thermotolerant, yet least abundant, Rca isoforms in cowpea will enable adaptation to leaf temperatures resulting from heatwaves that are more intense or accompanied by water deficit, which are likely to occur in sub-Saharan Africa.

Materials and Methods

Gene identification

Cowpea *Rca* genes were identified by searching the cowpea genome (Phytozome 12, cowpea genome v1.1) using keywords and known Rca protein sequences from *Arabidopsis thaliana*, *Nicotiana tabacum*, and *Triticum aestivum* (Supporting Information Table S1)(Goodstein *et al.*, 2012; Lonardi *et al.*, 2019). This identified 3 genes for *Rca* in cowpea: *Vigun01g219300* (*Rca1*), *Vigun08g150700* (*Rca8*), and *Vigun10g051600* (*Rca10*). Alignment with known sequences and key conserved features of canonical Rcas allowed identification of the products of each gene. Transit peptide sequences for each protein were identified by alignment to known Rca sequences (with known transit peptide locations). The analysis was repeated using the updated Phytozome 13 cowpea genome v1.2 and yielded identical Rca isoforms (Supporting Information Fig.S1). Analysis of transcript sequences showed that *Rca1* encodes a 384 amino acid (aa) mature protein consistent with a β isoform. *Rca8* encodes a 419 aa α isoform and a 295 aa isoform that is shorter than a regular β isoform and unlikely to be functional. *Rca10* encodes both a 419 aa α and a 382 aa β isoform by alternative splicing.

The cowpea *HSP20* (*Vigun06g052200*) gene, used as a heat stress marker, was identified as a homolog of the soybean *HSP20* (*Glyma.18g094600*) shown to be upregulated in two soybean cultivars exposed to heat stress (Song *et al.*, 2017). The Arabidopsis homolog (*At4G27670*) is also upregulated in heat stress (eFP Browser Stress Series, https://bar.utoronto.ca/)(Kilian *et al.*, 2007; Winter *et al.*, 2007). The *Glyma.18g094600* coding sequence was downloaded from SoyBase (https://legacy.soybase.org) and used to search the cowpea genome as above (Brown *et al.*, 2021).

Cloning of cowpea Rca coding regions and construction of *E. coli* expression vectors

Coding regions for the mature proteins of cowpea Rca1β, Rca8α, Rca10α and Rca10β were codon optimised for *E. coli, de novo* synthesised and subcloned into pUC57 (Kan^R) by Aruru Molecular Ltd. (Dundee, UK). A Golden Gate compatible *E.coli* expression vector was created from the pET His TEV LIC plasmid (a gift from Scott Gradia, Addgene plasmid #29653; http://n2t.net/addgene:29653; RRID:Addgene_29653). Ligation independent cloning was used to add a Golden Gate cassette taken from pICH47742 (part of the MoClo Toolkit that was a gift from Sylvestre Marillonnet, Addgene kit # 1000000044) into pET His TEV LIC, generating the new Golden Gate compatible pET His TEV GG plasmid (Weber *et al.*, 2011; Werner *et al.*, 2012). Cloning a coding region into this vector allows production of a target protein fused to an N-terminal histidine (His) tag that can be removed with TEV protease.

191 PCR was used to add Golden Gate overhangs to the four optimised *Rca* sequences (see
192 Supporting Information Table S2 for primers used). Golden Gate reactions (final volume 15
193 µL) were performed with a 2:1 molar ratio of insert:plasmid and the following reagents (final
194 concentration): 1× T4 DNA Ligase buffer, 0.1 mg mL^{-1} BSA, 1 mM ATP, 40 KU/mL T4 DNA
195 Ligase, 2 KU/mL *Bsa* I. All reagents from NEB, except ATP (Promega). Reaction conditions
196 were 30 cycles of [37 °C for 2 min followed by 16 °C for 3 min], 37 °C for 5 min, 80 °C for 10
197 min, and 16 °C for 1 min. 5 µL of the reaction mix was used to transform *E. coli* DH5α cells.
198 Resulting colonies were used to generate plasmid DNA for sequencing with primers T7F and
199 T7R (Source Bioscience) to verify correct sequence including in-frame fusion of the coding
200 region to the His tag.

201 Generation of *E. coli* expression strains

202 Expression constructs were used to transform BL21(DE3)pLysS *E. coli* competent cells
203 (Invitrogen). PCR and sequencing were used to confirm the presence of the correct
204 constructs in the BL21(DE3)plysS *E. coli* cells. Several cell lines were tested for each
205 construct to identify the cell strains with the highest expression levels for the target proteins.
206 Expression experiments were then scaled up for protein purification.

207 Recombinant Rca expression and purification

208 Starter cultures (10 mL M9ZB medium, containing kanamycin and chloramphenicol, both at
209 50 µg/mL) were inoculated from glycerol stocks and grown overnight at 37 °C with 225 rpm
210 orbital shaking. Dynamite medium (containing kanamycin and chloramphenicol, at 50 µg/mL)
211 was seeded with the overnight starter culture (10 mL starter culture in 1 L Dynamite
212 medium). This culture was grown for 3-4 h at 37 °C with shaking at 220 rpm until OD_{595}=0.6-
213 0.8 and then IPTG (0.5 mM final concentration) added to initiate protein expression. Cultures
214 were then transferred to 24 °C with 220 rpm shaking for 20 h. Cells were pelleted by
215 centrifugation (5,000 × *g*, 4 °C, 20 min), washed with 40 mL buffer (50 mM HEPES pH 7.2,
216 300 mM NaCl, 5 mM $MgCl_2$), transferred to 50 mL screw capped tubes before finally
217 collecting by centrifugation (5,000 × *g*, 4 °C, 20 min). The pellet was flash frozen in liquid
218 nitrogen and stored at -80 °C.

219 Cell pellets were thawed on ice and resuspended in Lysis Buffer (50 mM HEPES pH 7.2, 5
220 mM $MgCl_2$, 300 mM NaCl, 50 mM Imidazole, 0.1% Triton X-100 (v/v), 10 µM leupeptin, 1
221 mM PMSF), using 7 mL buffer for every 1 g of pellet. Cells were lysed on ice using a probe
222 sonicator and 5 cycles of 30 s on 30 s off until the solution was homogeneous. Cell debris
223 was removed by centrifugation (23,000 × *g*, 4 °C, 30 min) and the soluble fraction pushed
224 through a 0.45 µm syringe filter prior to chromatography.

225 Purification of the Rca protein was achieved using an NGC chromatography system (Bio-
226 Rad, UK), equipped with a nickel-charged IMAC column (1 mL HisTrap Fast Flow, Cytiva)
227 and a desalting column (10 mL Bio-Scale Mini Bio-Gel P6 Desalting Cartridge, Bio-Rad).
228 IMAC and desalting columns were equilibrated with Equilibration Buffer (5 mL: 50 mM
229 HEPES pH 8, 300 mM NaCl, 5 mM $MgCl_2$, 50 mM imidazole) and Final Buffer (13 mL: 50
230 mM HEPES pH 8, 5 mM NaCl, 5% glycerol), respectively. The sample was applied to the
231 IMAC column, followed by Wash Buffer (15 mL: 50 mM HEPES pH 8, 300 mM NaCl, 5 mM
232 $MgCl_2$, 125 mM imidazole). Bound protein was eluted using a higher concentration of
233 imidazole (2.1 mL: 50 mM HEPES pH 8, 300 mM NaCl, 5 mM $MgCl_2$, 300 mM imidazole)
234 and directly applied to the desalting column. Buffer was exchanged with 15 mL Final Buffer
235 and 1 mL fractions collected. Fractions containing protein were identified using a UV/Vis
236 detector reading at 280 nm. Fractions containing the highest protein concentration
237 (determined using Bradford reagent, BIO-RAD) were pooled, ATP and DTT (2 mM and 5
238 mM final concentration respectively) added and 50-100 µL aliquots frozen in liquid nitrogen
239 before storage at -80 °C.

240 *In vitro* characterization of thermal optima of Rca isoforms

241 The rate of ATP hydrolysis by Rca isoforms was assayed using the method described by
242 Chifflet *et al.* (1988), with modifications as described within Degen *et al.* (2020). ATP
243 hydrolysis was measured at a range of temperatures (20-55 °C) using 5-minute assays, with
244 reactions initiated through addition of Rca (final concentration 1 µM Rca monomer) and
245 quenched via addition of SDS. After quenching, all reactions and standards were kept at 4
246 °C until inorganic phosphate (P_i) determination. The P_i released during ATP hydrolysis was
247 determined by measuring the absorbance of molybdenum blue at 850 nm in a
248 spectrophotometer (SpectroStar Nano, BMG Labtech, UK).

249 Rubisco reactivation assays were conducted at a range of temperatures (20-45 °C) following
250 the procedures of Barta *et al.* (2011) and Degen *et al.* (2020). Briefly, Rubisco purified as per
251 Amaral *et al.* (2024) was used to prepare inhibited Rubisco complexes (ER) through
252 incubation with RuBP overnight at 4 °C. The two-stage reactivation assay comprises a first
253 stage assay where Rca is added to inhibited Rubisco (ER) at a test temperature (20-45 °C),
254 with aliquots from this assay taken at time intervals to initiate the second stage assay that
255 measures Rubisco activity. This Rubisco activity is a function of the Rca, time allowed for
256 reactivation, and the temperature of the first stage (Supporting Information Fig. S2). With
257 known quantities of Rca and Rubisco, and appropriate controls as detailed within Degen *et*
258 *al.* (2020), Rca reactivation of Rubisco can be established. Maximum Rubisco activity was
259 determined at every temperature and was comparable among assays with each of the four
260 Rca isoforms.

Independent purifications of each isoform were used as biological replicates. For ATPase activity, three biological replicates were measured for Rca8α and four for the each of the rest of the isoforms. For Rubisco reactivation, four biological replicates were measured for temperatures 20-32 °C and three for temperatures 38-45 °C. To estimate maximum ATP hydrolysis and Rubisco activation activities and the corresponding temperatures at which the maximum values are attained, second- to third-order polynomials and generalized additive models (GAM) were fitted to the experimental data using the gam function from the mgcv 1.8–24 package in R (Wood, 2017). The model that best fit the experimental data was selected based on the Akaike information criterion using the AIC function (Akaike, 1974) (Supporting Information Table S4). The selected model was fitted to each set of the biological replicates (Table 1) as well as the whole dataset (Supporting Information Table S3). T_{max} was calculated as the temperature corresponding to maximum activity. T_{opt} was calculated as the range where activity was maintained above 70% of maximum value. $T_{0.5}$ was calculated as the temperature where activity dropped below 50% of maximum value.

Plant material and growth conditions

Vigna unguiculata (L.) Walp. cv. IT97K-499-35 seeds (kindly provided by B.B. Singh) were germinated in 0.6 L Deepots (D40H, Stuewe & Sons) containing 1:1 (v:v) mixture of nutrient-rich compost (Petersfield Growing Mediums) and silver sand (horticultural grade, Royal Horticultural Society). Plants were grown in eight growth cabinets (MC1000, Snijders Labs) and watered as needed to soil saturation. Cabinets were maintained at day/night temperatures of 28/18 °C, 70% relative humidity and 400 ppm CO_2 concentration (control conditions). A 12 h photoperiod of constant light of 850 μmol m^{-2} s^{-1} at canopy level was maintained via LED lighting (NS1 spectrum, Valoya). Four cabinets were randomly selected to apply a heat treatment starting at 13 days after sowing (das) including an intermediate day with day/night temperatures of 34/24 °C followed by 5 days of 38/28 °C (Supporting Information Fig. S3a). Data loggers (OM-EL_USB-2, Omega Engineering Ltd.) were placed at canopy level in each cabinet to record temperature and relative humidity every 15 minutes (Supporting Information Fig. S3b).

Plant Growth and Sampling

Twenty cowpea plants were grown in each cabinet and sampled or measured for different analyses following a randomised design (Supporting Information Fig. S4). All samples and measurements were taken from the central leaflet of the first trifoliate leaf. Leaf disc samples were taken 4-5 h into the light period, after which plants were cut above the unifoliate leaves to reduce shading of neighbouring plants. Separate plants were used for sample collection in

295 subsequent time points. For non-destructive measurements, such as plant growth traits and
296 chlorophyll content, the same individuals were measured at all time points.

297 Growth measurements were obtained at 15, 17 and 22 das (days 2 and 4 of the heatwave
298 and on day 4 of the post-heatwave recovery period, Supporting Information Fig. S6). Leaf
299 chlorophyll content was estimated using a chlorophyll concentration meter (MC-100,
300 Apogee) by measuring 3 positions on the central leaflet for each plant. Plant height was
301 measured using a ruler from the soil level to the apical meristem. Leaf length and width
302 (widest part perpendicular to the length) were also measured with a ruler for the central
303 leaflet only. Leaf thickness was measured with a digitronic calliper 110-DBL (Moore &
304 Wright). Total above-ground biomass was determined on a separate set of plants by drying
305 leaves and stems at 60 °C until constant weight.

306 Chlorophyll fluorescence (method below) measurements were conducted every day of the
307 heatwave. Three 0.38 cm^2 leaf discs were excised and quickly placed with the adaxial
308 surface upwards on a single layer of wet filter paper on a thin plastic tray (<0.5 mm) and
309 immediately transported to the fluorescence imager.

310 A thermal imaging camera (CAT S60 smartphone, Caterpillar) was used prior to sampling to
311 assess T_{leaf}. Each image was later analysed with FLIR Thermal Studio software (Teledyne
312 FLIR LLC), providing the mean temperature across an area of the leaf surface (Supporting
313 Information Fig. S5).

314 For RNA-seq analyses (method below), four 0.55 cm^2 leaf discs were collected from 4
315 independent biological replicates per treatment per timepoint (days 1, 3 and 5 of heatwave)
316 using a cork borer, then immediately snap frozen in liquid nitrogen and stored at -80 °C.

317 For protein and Rubisco analyses, four 0.55 cm^2 leaf discs were excised as above and
318 quickly placed with the adaxial surface upwards on a single layer of wet filter paper to
319 maintain turgidity. The filter paper was contained in a thin plastic tray and positioned on the
320 surface of the water in a circulating water bath in the artificial sunlight simulation rig (Taylor
321 *et al.*, 2022). PPFD at leaf-disc-level was 850 µmol m^{-2} s^{-1}. Water bath temperature was
322 maintained at 26 °C or 32 °C (±0.1 °C) for control or heat-treated plants, respectively, to
323 mimic leaf temperatures in the growth cabinet. After 1 h incubation leaf discs were quickly
324 blotted on absorbent paper to remove excess moisture, then immediately frozen in liquid
325 nitrogen and stored at -80 °C.

326 For Rubisco reactivation in leaf extracts (LE), eight 0.55 cm^2 leaf discs were sampled on day
327 5 of the heatwave. A different plant was used for each of the seven temperatures of the

328 temperature response curve (20, 25, 32, 38, 40, 45 °C). Samples were quickly frozen in
329 liquid nitrogen, then stored at -80 °C until further analysis.

330 Determining T_{crit} via chlorophyll fluorescence

331 Samples were analysed using a chlorophyll fluorescence imager (closed 800C FluorCam,
332 Photon System Instruments). The imager contained a customized temperature-controlled
333 sample surface area which comprised an aluminium plate with imbedded copper piping
334 connected to a circulating temperature-controlled water bath (Optima TX150, Grant
335 Instruments). The filter paper was in contact with sponges which acted as water reservoirs to
336 ensure the paper remained wet during analysis (Supporting Information Fig. S7a). The
337 temperature of the sample surface area and leaf discs were recorded using type k
338 thermocouples and a data logger (RDXL4SD, Omega). Additional thermocouple wires were
339 placed in contact with the sample surface area, and extra leaf discs, to record temperature
340 throughout the analysis (Supporting Information Fig. S7a). Samples were first dark adapted
341 for 1 h at 26 °C. After dark adaptation, the Fv/Fm protocol in the software (FluorCam 7,
342 Photon System Instruments) was used to make measurements of the maximum quantum
343 efficiency of photosystem II over a range of temperatures. The temperature of the leaf discs
344 was used to assess when the measurement temperature had been reached and was stable.
345 Once stable, the temperature was held for 3 min before the Fv/Fm measurement was
346 taken.

347 The data for each set of three leaf discs from the same plant were averaged and plateauing
348 Fv/Fm points at higher temperatures were removed before the remaining data were used to
349 calculate T_{crit} (Supporting Information Fig. S7b) with the segmented function from the
350 segmented package(Muggeo, 2017) in R. This function uses a previously fitted linear model
351 to identify a breakpoint and fits two linear models before and after the breakpoint. The
352 breakpoint in the Fv/Fm curve was taken as T_{crit} while the slopes of the two linear models
353 were taken as m1 & m2 (Supporting Information Fig. S7b, c, d).

354 Protein extraction, Rubisco activity and content

355 Proteins were extracted from leaf disc samples and Rubisco activity assays were performed
356 in a randomised order, as described previously (Taylor *et al.*, 2022; Ashton *et al.*, 2024). The
357 activation state of Rubisco was calculated as the ratio of initial to total activity. In short,
358 aliquots of the leaf extract supernatant were added to an assay mix containing $^{14}CO_2$ and
359 RuBP to initiate assays that gave an estimate of Rubisco initial activity, whereas Rubisco
360 total activity was measured after allowing a 3-minute incubation period of the leaf extract in
361 the assay mix without RuBP to allow full carbamylation of Rubisco.

362 Aliquots of leaf extract supernatant were also used for determining Rubisco content via ^{14}C-
363 CABP (2-carboxy-D-arabinitol 1,5-bisphosphate) binding, as previously described (Ruuska
364 *et al.*, 1998; Ashton *et al.*, 2024) and total soluble protein content, using the Bradford method
365 (Bradford, 1976).

366 RNA extraction, RNA-seq and RT-qPCR

367 Frozen leaf disc samples were ground to a fine powder in liquid nitrogen using a pestle and
368 mortar. Total RNA was extracted from 20-30 mg tissue using a NucleoSpin™ RNA Plant Kit
369 (Macherey-Nagel) including a DNase treatment, according to the manufacturer's
370 instructions. RNA concentration and quality were determined by spectrophotometry using a
371 microplate reader and LVis plate (SPECTROstar Nano, BMG Labtech) (Supporting
372 Information Table S5). Further QC analysis of RNA samples was performed by Novogene
373 using a Qubit fluorometer (Invitrogen) and an Agilent 5400 fragment analyzer, followed by
374 mRNA purification (using poly-T oligo-attached magnetic beads), library construction and 2 x
375 150 bp paired-end (PE150) sequencing using an Illumina NovaSeq 6000 (read depth of 30
376 million reads).

377 An initial filtering was applied to the raw data to remove reads containing adapters,
378 containing N > 10% (N represents bases that cannot be determined) and low-quality bases
379 (Phred < 5). Further read quality assessment and trimming was performed using the FastQC
380 tool, version 0.12.1 (http://www.bioinformatics.babraham.ac.uk/projects/fastqc/) and
381 cutadapt, version 4.2 (Martin, 2011). Low quality bases (Phred < 30) were trimmed from 3'
382 ends of each read, flanking N bases were removed and trimmed reads shorter than 50 bp
383 were discarded (for sequencing and alignment statistics see Supporting Information Table
384 S6).

385 Cowpea IT97K-499-35 reference transcriptome v1.2 (Lonardi *et al.*, 2019; Liang *et al.*, 2024)
386 was downloaded from Phytozome 13 (Goodstein *et al.*, 2012). Salmon, version 1.10.1 (Patro
387 *et al.*, 2017) was first used to index the reference transcriptome and then quantify expression
388 of clean reads at the transcript level. To identify changes in the cowpea Rca transcripts TPM
389 values were extracted from the Salmon Quant.sf output files for Rca, RbcS and HSP20
390 transcripts. Three transcripts are present for Rca1β (the first two result in the same protein,
391 the third is missing some of the N domain) and TPM values for all three were combined.
392 Three transcripts exist for Rca8α (transcripts 2 and 3 are non-functional and have low
393 expression) so here we only present data for the first transcript. For Rca10 transcripts 1, 3
394 and 4 are combined to give total expression for the alpha isoform and transcript 2 alone
395 represents the beta isoform. The three transcripts for RbcS were also combined.

Global gene expression analysis was carried out in R version 4.4.1 (2024-06-14, Race for Your Life). Raw counts from Salmon were loaded into EdgeR 4.2.1 using tximport 1.32.0 and rtracklayer 1.64.0. Transcript data for each gene was combined at this stage so that all global analysis was performed at the gene-level. PCA plot was made using logCPM the PCAtools 2.16.0 to check that biological replicates group together and to look for outlying samples. Here we used the counts per million (CPM) to remove the variability due to library depth. The EdgeR trimmed mean of M-values (TMM) method was used for normalisation of read counts. The data was filtered using a CPM threshold to remove genes with zero or near zero expression. A generalised linear model was then fitted to the normalised and filtered data for each gene. Empirical Bayes quasi-likelihood F-tests were used to test whether genes were significantly differentially expressed between heat-treated and control plants on each day of the heatwave. To control for multiple testing, p-values were calculated using the false discovery rate (FDR) of Benjamini-Hochberg. Differentially expressed genes (DEGs) were then identified using the threshold values of a false discovery rate (FDR) of < 0.05 and a log2 (|fold change|) of >1.5.

Rca gene expression changes were validated via RT-qPCR (Supporting Information Fig. S11). For sampling and detailed methodology see Supporting Information Tables S7 & 8.

Rca isoform quantification via western blotting

To quantify the abundance of different Rca protein isoforms, an aliquot of supernatant resulting from Rubisco analysis was mixed with SDS-PAGE loading buffer and separated as previously described on Perdomo *et al.* (2018) on a 12% TGX Stain-Free gel (Bio-Rad). Gels were imaged to assess total protein before transfer to a nitrocellulose membrane using a dry blotting system (iBlot2, Thermo Fisher Scientific). Membranes were stained with REVERT Total Protein Stain for normalisation (Li-Cor Biosciences) and imaged prior to application of antibodies. To compare the abundance of α and β isoforms of Rca, an antibody with broad specificity for both isoforms was used (Feller *et al.*, 1998,a gift from Michael Salvucci), with detection via a secondary fluor-tagged antibody (IRDye800CW, Li-Cor Biosciences, RRID:AB_1660973). A dilution series of a pooled sample was run on every gel alongside the samples to verify antibody detection was within the linear range. To quantify Rca8α, a more specific antibody was used (Abcalis) in place of the broad specificity antibody. The anti-Rca8α specific antibody was generated using phage display with the peptide selected targeted against KRGAFYGKAAQQINVP (amino acid residue 376-391), as described in Bloemers & Carmo-Silva (2024). All blot images were obtained using an Odyssey FC (Li-Cor Biosciences). Empiria studio software (version 2.3.0.154, Li-Cor Biosciences) was used for image data analysis and normalisation with the total protein stain, with values determined as signal intensity.

Characterization of Rca thermal optima in leaf extracts

Rubisco reactivation by Rca in leaf extracts was determined as described in Carmo-Silva & Salvucci (2011). Eight leaf discs per plant were sampled from the youngest fully expanded leaf on day 5 of the heatwave. Separate samples were used for assaying each of the seven temperatures of the temperature response curve shown in Fig. 4, and eight plant sample replicates were used per temperature. Samples were stored at -80 °C until further analysis. One replicate of samples from one cabinet at control and one cabinet at high temperature was used in each day of Rca assays, with samples allocated randomly to each assay temperature. Supporting Information Fig. S14 illustrates the method which uses leaf extracts as the source of both Rubisco and Rca, incubates sub-aliquots with different assays mixes, and then carries out a two-stage assay very similar to the assay with the purified proteins. This enables determination of the capacity of a population of Rca, drawn from plants grown in different conditions, to reactivate Rubisco. Model fitting and temperature parameter (T_{max}, T_{opt} and $T_{0.5}$) calculations were conducted as described for the *in vitro* Rca activity assays above. From the same samples, aliquots of leaf homogenate were used for leaf chlorophyll content determination as described previously in Sales *et al.* (2022) and Taylor *et al.* (2020), according to equations by Lichtenthaler (1987). Aliquots of the desalted extract were used for total soluble protein (TSP) content determination using the Bradford method (Bradford, 1976). Results are presented in Supporting Information Table S3.

Data analysis

Geneious 2024.0.7 was used to generate protein alignments depicted in Fig. 1a. Data was processed using R 4.3.1 and RStudio 2024.09.0. Graphs were prepared using the ggplot 2 (Wickham, 2017), EnhancedVolcano (Blighe *et al.*, 2018), VennDiagramm (Chen, 2022), ggpubr (Kassambara, 2023) and patchwork (Lin Pedersen, 2024) R packages. Outliers were detected with the Outliers package using Tukey's fences method, where outliers are defined as extreme values that are 1.5 times the interquartile range (1.5 IQR) below the first quartile or 1.5 IQR above the third quartile. Box plots show medians and the first and third quartiles (25th and 75th percentiles), and whiskers extend from the hinge to the largest or smallest value. Symbols represent individual data points (technical or biological replicates defined for each plot either on methods or figure legend). Bar plots show means and error bars represent standard error. For statistical analysis, normality of data was assessed using the Shapiro-Wilk test and equality of variances using the Levene test. For measurements on multiple days, two-way ANOVA tests were applied to determine if there were significant day, treatment or interactive effects, followed by post-hoc Tukey tests for multiple comparisons with Bonferroni correction. Compact letters display (cld) were generated after the post-hoc pairwise comparisons using packages mutlicomp (Bretz *et al.*, 2016) and multicompView

(Graves *et al.*, 2024). In cases where there was a slight violation of normality or homogeneity of variance when data between different days was compared, two-way ANOVA was still chosen as the most robust method. If normality and variance were severely violated, data was log transformed, and two-way ANOVA was applied to the transformed data provided assumptions were not severely violated in the transformed data. For measurements taken at a single timepoint (growth parameters), t-test was used to determine statistical significance between treatments. Statistical analysis results and full datasets are provided in the Source Data file.

Results

Cowpea contains four Rubisco activase isoforms

The cowpea genome contains three genes that encode Rca. The gene on chromosome 1 (*Vigun01g219300)* encodes an Rca β, the gene on chromosome 8 (*Vigun08g150700)* an Rca α, and the gene on chromosome 10 (*Vigun10g051600)* encodes both Rca α and β isoforms via alternative splicing (Fig. 1a). The gene on chromosome 8 also encodes a truncated version of Rca, however this would not produce a canonical, fully functional Rca as it has a premature stop codon before the α-helical domain which is necessary for the recognition of Rubisco by Rca (Portis *et al.*, 2008). Rca isoforms in cowpea exhibit minor sequence differences, primarily in the N-terminal region (the flexible domain critical for Rubisco binding) (Stotz *et al.*, 2011; Shivhare *et al.*, 2019, p. 20) and the α-helical domain (Supporting Information Fig. S1). These variations may contribute to functional diversity of Rca in cowpea, potentially allowing for fine-tuning of responses to different environmental conditions.

Cowpea Rca isoforms differ in thermal optima of activity *in vitro*

Previous studies have shown the potential for intraspecies variation of Rca thermal optima (Degen *et al.*, 2020). With four distinct isoforms in cowpea and its known ability to grow in warm (20-37 °C) temperatures (Barros *et al.*, 2021), recombinant versions of each isoform were produced for *in vitro* characterisation of cowpea Rca thermal optima (Fig. 1b). Both enzyme activities were assessed, i.e., the ability to reactivate inhibited cowpea Rubisco and the ATPase activity that drives reactivation (Robinson & Portis, 1989). Rubisco reactivation by Rca was calculated after accounting for the spontaneous reactivation of Rubisco, expressed as a percentage of maximum Rubisco activity. The spontaneous reactivation of Rubisco, although insignificant at lower temperatures, increases with temperature (Supporting Information Fig. S2) as the Rubisco catalytic site becomes more flexible. For all the Rca isoforms, the temperature corresponding to the peak of activity (T_{max}), the range of temperatures at which activity was maintained above 70% of the maximum value (T_{opt}) and the temperature at which activity drops below 50% of the maximum ($T_{0.5}$) were consistently higher for ATPase activity than for Rubisco reactivation activity (Table 1). A higher sensitivity of Rubisco reactivation compared to ATP hydrolysis has been previously reported and may be due to the interaction with Rubisco being the key step impacted by elevated temperatures in Rca (Degen *et al.*, 2020). It has also been shown that while ATP hydrolysis can be catalysed by Rca oligomers consisting of three subunits, Rubisco reactivation requires oligomers containing more than three subunits (Keown *et al.*, 2013; Hazra *et al.*, 2015).

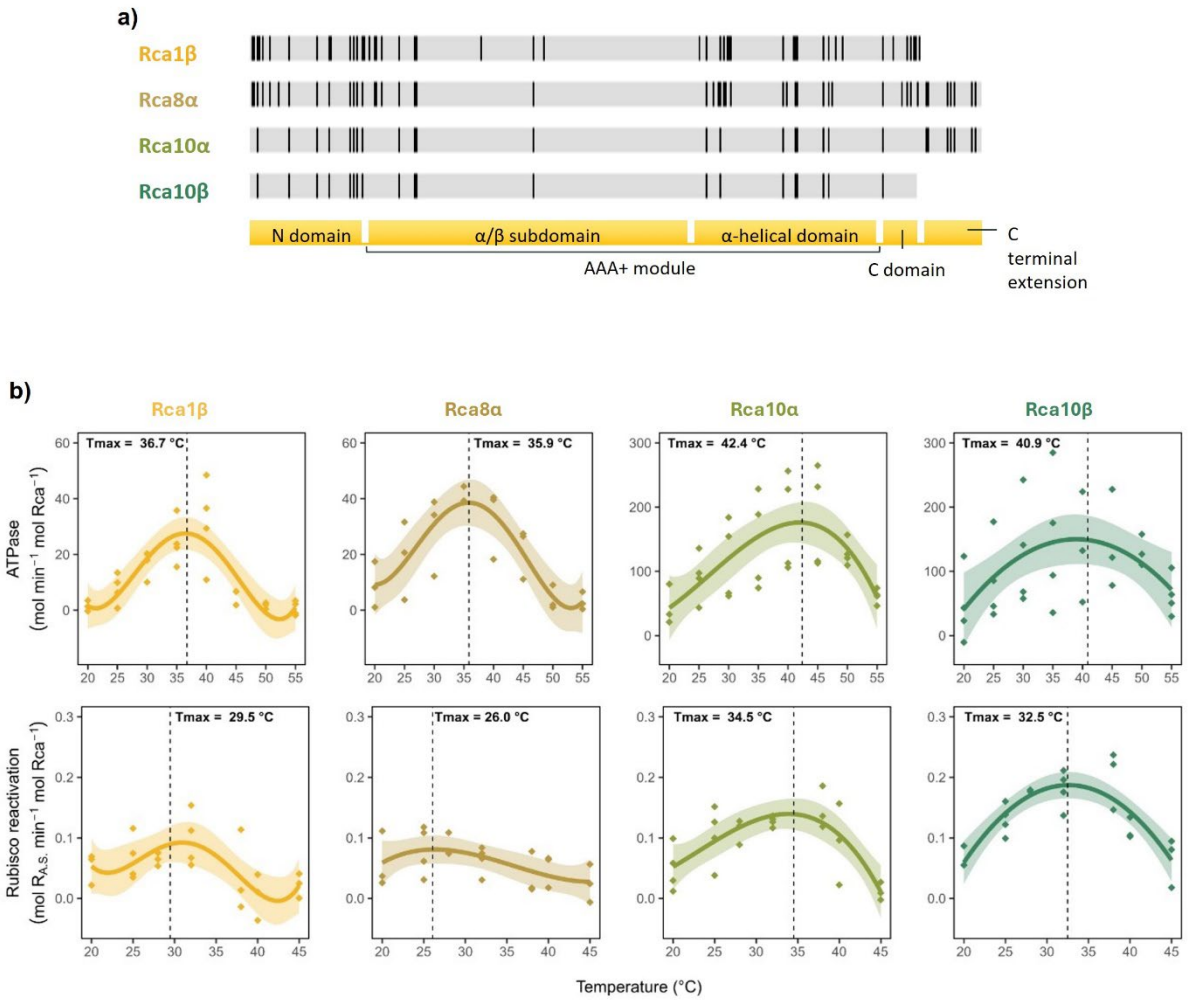

510

511 **Figure 1. Temperature response of cowpea Rca isoforms in vitro.** a) Amino acid residue
512 alignment of the four cowpea Rca isoforms encoded by genes located on chromosomes 1, 8
513 and 10. Black vertical lines indicate differences in sequence among the genes. The following
514 corresponding regions of the protein are shown: N-domain, α/β subdomain, α-helical
515 domain, C-domain, and C-terminal extension. b) Temperature response of ATP hydrolysis
516 and Rubisco activation by cowpea Rubisco activase isoforms *in vitro*. Rate of ATP hydrolysis
517 and Rubisco reactivation by recombinantly produced purified cowpea Rca isoforms Rca1β,
518 Rca8α, Rca10α and Rca10β. Assays were performed at the indicated temperatures using 1
519 μM purified Rca and 5 mM ATP. Activation of pre-inhibited Rubisco used 5 μM Rubisco
520 active sites ($R_{A.S.}$) in the ER form (1:5 Rca:$R_{A.S}$). Rubisco activation is presented relative to
521 maximum Rubisco activity, determined as the Rubisco activity when Rca is allowed to
522 reactivate inhibited Rubisco for 5 min. Values represent biological replicates (independent
523 purifications; n=3-4 biological replicates). Lines represent the best fit for each enzyme
524 (selected by the Akaike information criterion) and shaded areas denote the 95% confidence
525 interval for each fit (Supporting Information Table S4). Full sample data are provided in the
526 source data file.

527 **Table 1.Temperature response of *in vitro* Rubisco activase (Rca) activity.** Maximum
528 rate of ATP hydrolysis and Rubisco activation and corresponding temperature (T_{max}),
529 optimum temperature range (T_{opt}, above 70% activity) and temperature above the optimum
530 at which 50% of the maximum activity remains ($T_{0.5}$). Values were estimated from best-fit
531 models that describe the *in vitro* temperature response of each Rca isoform (Supporting
532 Information Table S4). The best-fit model was applied to each of three biological replicates
533 with complete temperature response curves shown in Fig. 1b. The first biological replicate
534 was excluded from the fitting of the individual replicates because the temperature response
535 of Rca activity was incomplete (determined only up to 32°C); this replicate is included in the
536 model fitting to the complete temperature response data set (Supporting Information Table
537 S3). Values show here are the mean ± standard error of the mean of values determined for
538 individual replicates of temperature response curves (n=3).

Rca Isoform	$ATPase_{max}$ (mol min^{-1} mol Rca^{-1})	T_{max} (°C)	T_{opt} (°C)	$T_{0.5}$ (°C)
1β	28.0 ± 5.3	36.7 ± 0.5	29.9 – 43.4	43.4 ± 1.1
8α	35.9 ± 8.1	35.9 ± 0.7	28.4 – 43.1	45.6 ± 0.2
10α	179.0 ± 36.8	42.6 ± 1.1	30.9 – 51.6	53.6 ± 0.7
10β	183.4 ± 58.5	40.9 ± 1.1	28.5 – 52.1	53.5 ± 0.3
Rca Isoform	**$Rubisco\ reactivation_{max}$ (mol $R_{A.S.}$ min^{-1} mol Rca^{-1})**	**T_{max} (°C)**	**T_{opt} (°C)**	**$T_{0.5}$ (°C)**
1β	0.10 ± 0.03	29.5 ± 1.2	27.7 – 34.4	36.1 ± 1.5
8α	0.09 ± 0.02	26.0 ± 2.9	22.1 – 36.0	41.0 ± 2.9
10α	0.14 ± 0.01	34.5 ± 1.0	26.5 – 40.8	42.4 ± 0.2
10β	0.19 ± 0.01	32.5 ± 0.4	24.0 – 40.9	43.3 ± 0.8

539

540 The two Rca isoforms encoded by *Rca10* were faster at hydrolysing ATP and reactivating
541 Rubisco, had higher thermal maxima (T_{max}), broader thermal optima (T_{opt}), and showed
542 thermal sensitivity ($T_{0.5}$) at warmer temperatures compared to the other two isoforms (Fig.
543 Fig. 1b;Table 1). T_{max}, T_{opt}, and $T_{0.5}$ calculated for both ATP hydrolysis and Rubisco
544 reactivation were generally similar for Rca1β and Rca 8α (Table 1), but Rca1β exhibited the
545 lowest $T_{0.5}$ for reactivation activity (36.1 ± 1.5 °C). Up to 34 °C, all Rca isoforms maintained
546 at least 70% of maximum Rubisco reactivation activity. Rca10α exhibited the highest
547 temperature corresponding to the peak of activity for both ATP hydrolysis (T_{max} = 42.6 ± 1.1
548 °C) and Rubisco reactivation (T_{max} = 34.5 ± 1.0 °C). T_{max} values for Rca10α and Rca10β
549 were at least 3 °C higher for both ATP hydrolysis and Rubisco reactivation relative to Rca1β
550 and Rca8α (Table 1). Combined, the results show that the cowpea Rca10α and Rca10β
551 isoforms have faster rates, higher thermal maxima, broader thermal optima, and are less
552 sensitive to warmer temperatures than Rca1β and Rca8α.

553 A 5-day heatwave of +10 °C causes mild heat stress in cowpea

554 To investigate heat-induced changes in cowpea Rca *in planta*, young plants were exposed
555 to a 5-day heatwave consisting of an increase of 10 °C during both day and night. Plants
556 were cultivated for two weeks at 28/18 °C day/night, then in half of the controlled
557 environment cabinets the temperature was increased to 34/24 °C day/night for one day and
558 subsequently to 38/28 °C day/night for five days (Fig. 2a, Supporting Information Fig. S3, 4).
559 The intermediate day aimed to resemble a gradual increase in temperature in field
560 conditions. Plants were well watered throughout the heatwave as the focus was on the
561 impact of heat on Rca and we wanted to avoid confounding effects of water deficit on CO_2
562 diffusion and assimilation. Cabinet and leaf temperatures were monitored throughout the
563 experiment to ensure the plants were under heat stress conditions, with heat-treated plants
564 showing a 6 °C increase in leaf temperature to 32 °C (Fig. 2a, Supporting Information Fig.
565 S5). Thus, plants experiencing the heatwave had leaf temperatures within the T_{opt} of Rca
566 activity.

567 Plant growth traits were determined four days after the heatwave, after plants were allowed
568 to recover, and showed that the 5-day heatwave of +10 °C had only a mild impact on
569 cowpea (Fig. 2b). Exposure to elevated temperature resulted in decreased leaf thickness
570 and increased plant height; however, no effect on aboveground dry biomass was observed.
571 Total chlorophyll also decreased in leaves that had been exposed to heat when determined
572 four days after the heatwave (Fig. 2b). Measurement of leaf and plant traits during the
573 heatwave suggested an initial increase in the rate of cowpea leaf and plant growth (day 2,
574 Supporting Information Fig. S6), but only minimal differences between control and heat at
575 the end of and after the heatwave.

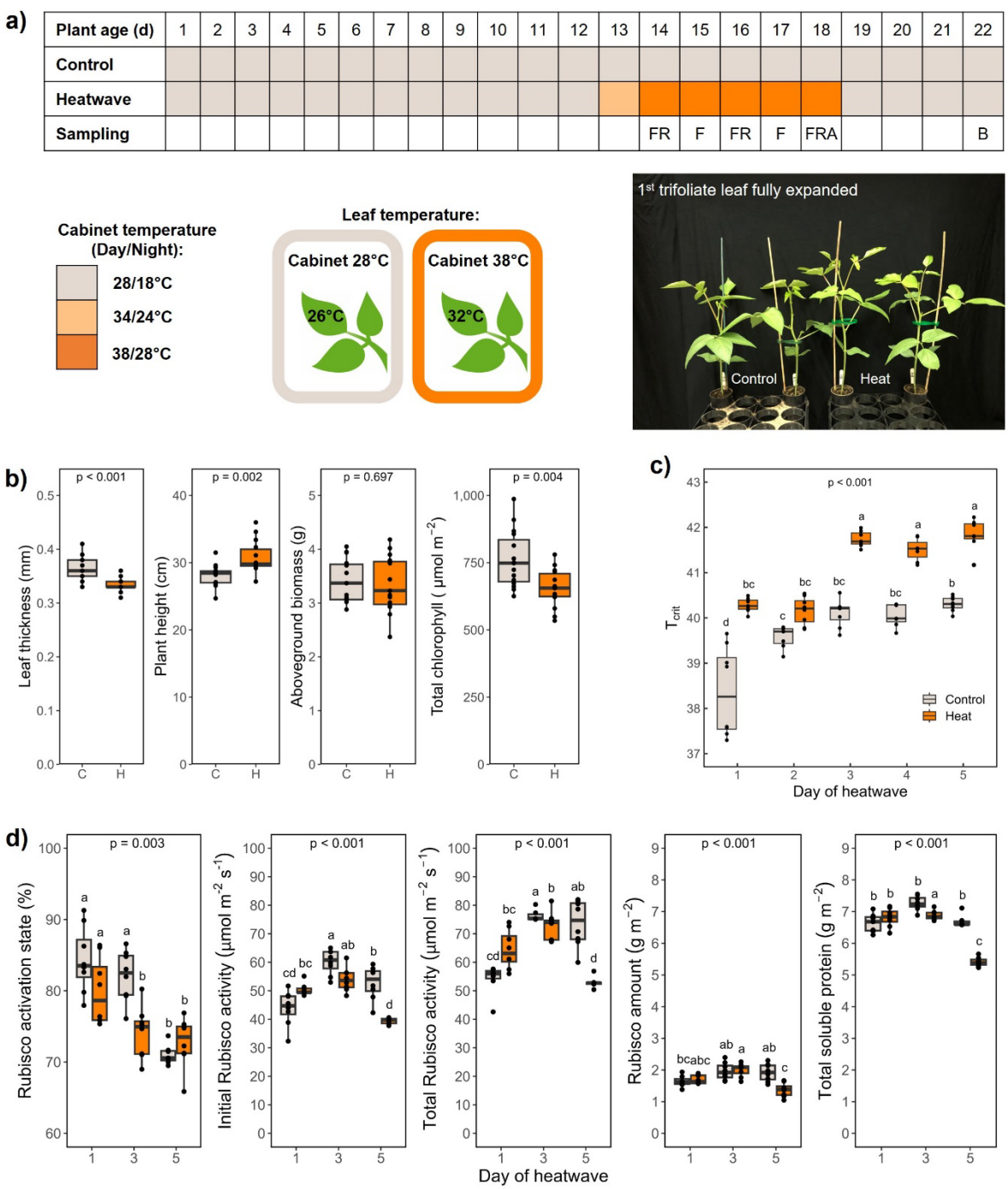

Figure 2. Cowpea response to a heatwave in controlled environment. a) Experimental design, heatwave and sampling times. Plants were grown at 28/18 °C day/night for 13 days, then exposed to an intermediate heat treatment for a day at 34/24 °C day/night before being exposed to a 38/28 °C day/night heatwave for five days. Sampling: (F) photosystem II maximum efficiency (Fv/Fm) was measured daily during the heatwave; (R) leaf discs for RNA-seq analysis, total soluble protein (TSP), Rubisco activity and amount were sampled on days 1, 3 and 5 of the heatwave; (A) samples for Rca temperature response in leaf extracts were taken on day 5 of heatwave; (B) growth parameters and biomass were measured on

585 day 22 of plant growth, four days after the end of the heatwave. Cabinet and leaf
586 temperature were monitored daily. b) Leaf and whole plant growth parameters were
587 measured four days after the end of the heatwave (n=15). Relative chlorophyll content was
588 determined using a concentration meter based on leaf reflectance. c) T_{crit} was calculated for
589 each day of the heatwave as the breaking point where the two Fv/Fm slopes meet
590 (Supporting Information Fig. S7). d) Rubisco activation state (n=7-8), (b) initial (n=7-8) and
591 (c) total activity per leaf area (n=6-8), Rubisco amount (n=7-8) and total soluble protein
592 (TSP; n=6-8) were measured in leaf extracts on days 1, 3 and 5 of the heatwave. P-values
593 were calculated using two-way ANOVA followed by Tukey post-hoc tests. Full sample data
594 are provided in the source data file.

595

596 As a proxy for photosynthetic activity, photosystem II (PSII) maximum efficiency (Fv/Fm) was
597 monitored throughout the heatwave (Supporting Information Fig. S7). Changes in Fv/Fm
598 indicate modifications in the functionality of PSII reaction centres, with a decrease indicating
599 photooxidative damage and reduced photochemistry quantum yield(Murchie & Lawson,
600 2013). Fv/Fm data collected from plants throughout the heatwave enabled determination of
601 T_{crit} (Fig. 2c), which corresponds to the temperature at which chlorophyll *a* fluorescence rises
602 rapidly in response to temperature due to thermal damage in PSII, and is used as an
603 indicator of photosynthetic thermal stability (Perez & Feeley, 2020; Posch *et al.*, 2022). In
604 heat-treated cowpea, Fv/Fm did not decline compared to control plants (Supporting
605 Information Fig. S7e), indicating that no irreversible damage was caused to PSII reaction
606 centres due to heat stress. In fact, heat-treated plants showed a progressive increase in the
607 temperature at which Fv/Fm decreased, resulting in a significantly higher T_{crit} after 3 days,
608 denoting increased PSII thermal stability ($p < 0.001$, Fig. 2c). These results indicate a
609 dynamic response that allows for PSII efficiency to adapt to warmer conditions.

610 Heat stress induces a decline in Rubisco activation state

611 In contrast to T_{crit}, the activation state of Rubisco decreased with heat treatment (Fig. 2d).
612 Importantly, a decline in Rubisco activation was observed from the beginning to the end of
613 the experiment as leaves aged. This decline was observed earlier in heat-treated plants (day
614 3) compared to control plants (day 5), indicating that heat stress accelerated this decline in
615 Rubisco function. Rubisco activation state, defined as the ratio of initial to total Rubisco
616 activity, reflects the enzyme's operational efficiency under different conditions. Initial activity
617 represents the enzyme's immediate functionality upon extraction, while total activity reflects
618 its potential after full carbamylation (Ashton *et al.*, 2024). Although Rubisco activation state
619 was similar on day 5, the initial and total activity was significantly lower in heat-treated

620 compared to control plants ($p < 0.001$, Fig. 2d). This decrease in Rubisco activity on day 5
621 of the heatwave was associated with decreased Rubisco amount and TSP (Fig. 2d), as no
622 significant differences were detected in Rubisco specific activity, expressed per quantity of
623 Rubisco protein (Supporting Information Fig. S8).

624 Heat stress induces the expression of thermotolerant Rca isoforms

625 Potential heat-induced changes in gene expression of *Rca* isoforms were assessed through
626 RNA sequencing analysis (RNA-seq) on days 1, 3 and 5 of the heatwave. A principal
627 component analysis (PCA) distinguished gene expression changes caused by heat stress
628 and those resulting from leaf aging (Fig. 3a, Supporting Information Fig. S9). Heat-induced
629 differential gene expression occurred from the first day of the heatwave, with both up and
630 down-regulation of genes evident in heat-treated plants compared to control conditions
631 throughout the duration of the heatwave (Supporting Information Fig. S9). Heat stress was
632 confirmed by upregulation of the heat shock protein *HSP20* (Song *et al.*, 2017) from day 1 of
633 the heatwave (Fig. 3b). The heatwave also decreased expression of the Rubisco small
634 subunit (*RbcS*), which is likely associated with the lower Rubisco amounts (Fig. 2c).

635 Under control temperature conditions, *Rca1β* was found to be the most abundant Rca
636 transcript, followed by *Rca8α*, while *Rca10α* and *Rca10β* were expressed at much lower
637 levels (Fig. 3c). Of the hundreds of up and downregulated genes (Supporting Information
638 Fig. S9), volcano plots showed that *HSP20* and *Rca10* were both upregulated on days 1, 3,
639 and 5 of the heatwave (Supporting Information Fig. S10). Heat-treated plants showed a
640 (non-significant) tendency for lower *Rca1β* expression, whereas *Rca8α*, *Rca10α* and
641 *Rca10β* were all upregulated during the heatwave (Fig. 3c). It is noteworthy that despite the
642 upregulation of both *Rca10* transcripts, their expression levels remained much lower than
643 *Rca1β* and *Rca8α* (Fig. 3c). Changes in *HSP20* and the four *Rca* transcript levels were also
644 confirmed via RT-qPCR (Supporting Information Fig. S11). Moreover, promoter analysis
645 revealed multiple stress responsive elements in *Rca1β and Rca8α*, while *Rca10* contains
646 two heat stress response elements and has fewer other stress responsive elements
647 (Supporting Information Fig. S12).

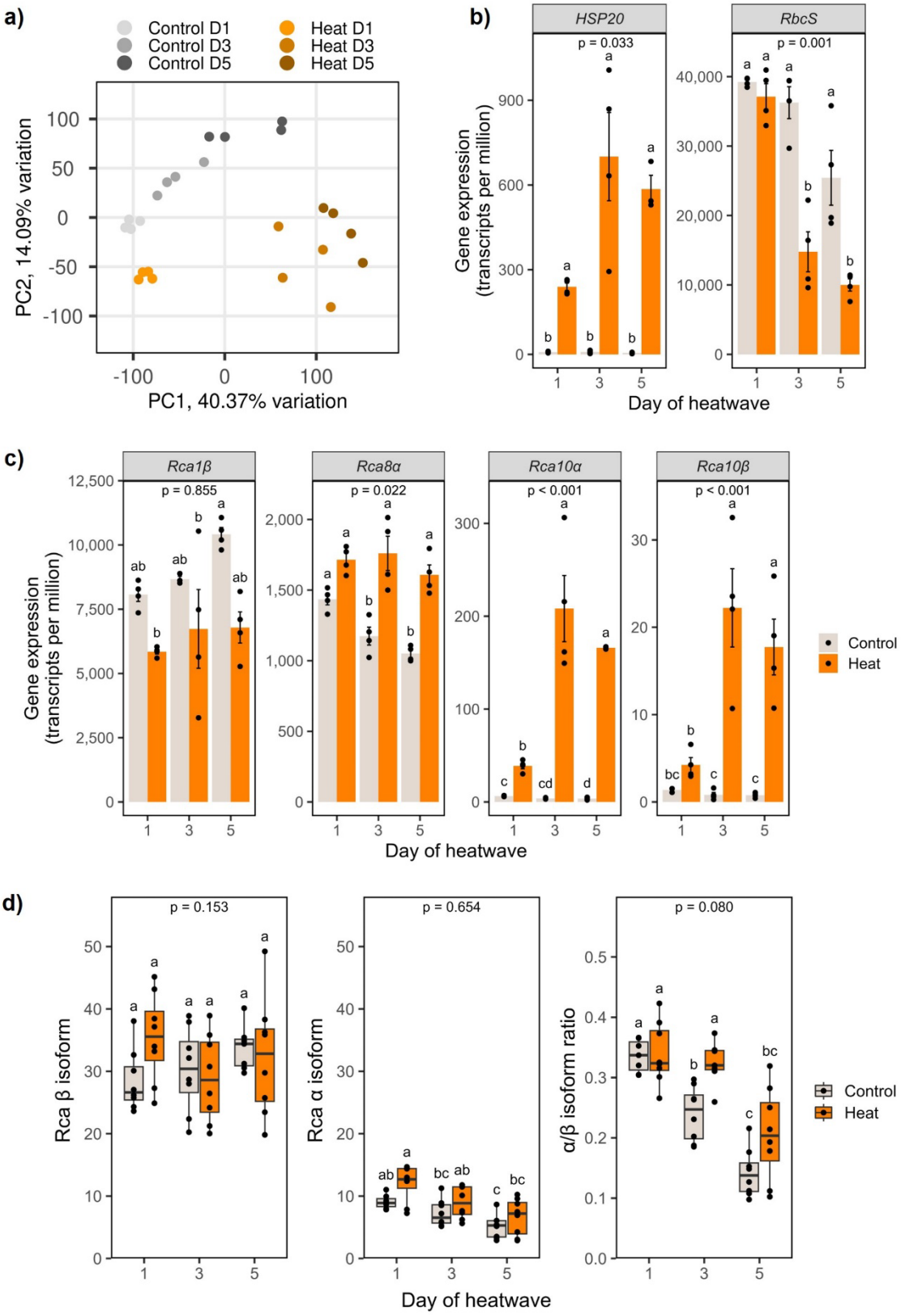

Figure 3. Differential gene expression and Rca protein abundance in cowpea during a heatwave. a) Principal components (PCA) plot of gene expression in leaves of heat-treated and control cowpea plants on days 1, 3 and 5 of the heatwave. b) Expression levels of the

652 heat shock protein 20 (HSP20) and the small Rubisco subunits (RbcS) were used as
653 reference. Bar plots represent means and error bars standard error. c) Expression levels of
654 the four cowpea Rca isoforms in control and heat-treated plant on days 1, 3 and 5 of the
655 heatwave (n=4). d) Protein abundance of Rca isoforms in leaves of control and heat-treated
656 plants on days 1, 3 and 5 of the heatwave (relative units). Rca α and β isoforms were
657 detected using an anti-Rca antibody and normalised to total protein. The size difference
658 between the α (45 kDa) and β (41 kDa) isoforms enabled the identification as separate
659 bands, and the estimation of the α/β ratio. P-values were calculated using two-way ANOVA
660 followed by Tukey post-hoc tests. Samples were run in separate gels and normalised to total
661 protein via reversible staining of the membrane. Blot images and full sample data are
662 provided in the source data file.

663

664 To investigate if changes in gene expression are reflected at protein level, the abundance of
665 leaf Rca protein was quantified via immunoblotting (Fig. 3d). A pan-Rca antibody that reacts
666 with all isoforms of Rca and enables quantification of Rca α and Rca β isoforms, as these
667 run separately in gel electrophoresis due to the difference in molecular weight, was used to
668 identify changes in abundance between α and β isoforms (Perdomo *et al.*, 2018). Whilst
669 differential gene expression was observed, changes in Rca protein were less pronounced.
670 As *Rca10β* transcript levels are almost negligible compared to *Rca1β*, it is reasonable to
671 infer that the β isoform protein is predominantly attributable to *Rca1β* expression. Expression
672 of *Rca8α* is also likely to produce most of the α isoform protein. Rca β remained unchanged
673 during the heatwave, while the α isoform decreased from day 1 to day 5 but was not
674 significantly different between control and heat-treated plants (Fig. 3d). Protein abundance of
675 Rca8α was also determined using a specific antibody that only reacts with this isoform
676 (Bloemers & Carmo-Silva, 2024). Rca8α showed a near identical pattern to the pan-Rca
677 antibody for Rca α with a non-significant tendency for increased abundance in heat treated
678 plants compared to the control (Supporting Information Fig. S13a). A significant increase in
679 the α/β ratio was however detected in day 3 of the heatwave, which may indicate differences
680 in the relative abundance of Rca isoforms (Fig. 3d). Due to their very low abundance,
681 Rca10α & Rca10β protein isoforms were undetected in leaf extracts with Rca10 specific
682 antibodies (Supporting Information Fig. S13b).

683 Heat-treated plants maintain Rca rate and thermal optimum

684 To test the hypothesis that heat-induced changes in the relative abundance of Rca isoforms
685 are reflected in activity, we characterised the temperature response of Rubisco reactivation
686 by Rca in protein extracts from leaves sampled on day 5 of the heatwave (Fig. 4). Leaf

extracts were desalted to produce the free Rubisco apoenzyme (uncarbamylated form), which was subsequently inhibited through incubation with RuBP (Carmo-Silva & Salvucci, 2011). The inhibited Rubisco in the leaf extract was then used to determine the rate of reactivation by the Rca holoenzyme via removal of RuBP from uncarbamylated Rubisco catalytic sites, at a range of temperatures (Supporting Information Fig. S14). Concurrent measurement of spontaneous reactivation of Rubisco in the absence of ATP, which is required for Rca activity, enabled calculation of the spontaneous (Supporting Information Fig. S15) and Rca-mediated rate of Rubisco reactivation (Fig. 4).

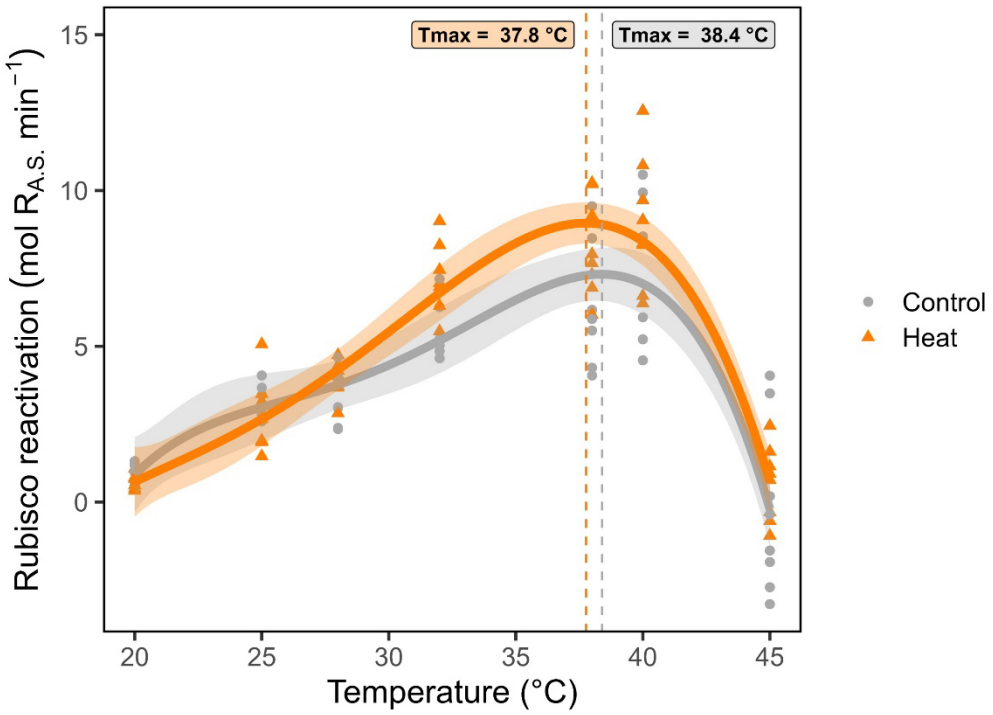

Figure 4. Temperature response of Rca activity in leaf extracts of control and heat-treated cowpea plants. Leaf discs were sampled on day 5 of the heatwave. The Rubisco and Rca contained in the leaves of each plant were extracted, Rubisco was inhibited by binding of RuBP to decarbamylated catalytic sites in the absence of CO_2 and Mg^{2+}, then reactivation by Rca was measured at varying temperatures by comparing an assay in presence of ATP and ATP-regenerating system with the negative control assay in the absence of ATP. The rate of Rubisco reactivation was calculated from measurements of Rubisco activity at 30 and 90 s after the start of the assay and expressed relative to maximum Rubisco activity in the same leaf extracts (as described in Supporting Information Fig. S14). Symbols represent biological replicates (leaf extracts from independent plant samples; n=8). Lines represent the best fit for each group of plants (selected by the Akaike information criterion) and coloured areas denote the 95% confidence interval for each fit (Supporting Information Table S9). Full sample data are provided in the source data file.

709

710 Rubisco reactivation by Rca tended to be faster in heat-treated compared to control plants,
711 however this increase was not statistically significant ($p > 0.05$, Fig. 4). Heat-treated plants
712 exhibited similar thermal optima of Rubisco reactivation by Rca to control plants at
713 approximately 38 °C (Table 2). T_{opt} and $T_{0.5}$ were also similar between control and heat-
714 treated plants (Table 2), indicating that the large fold-change in *Rca10* transcript abundance
715 (Fig. 3c) and the small change in heat-induced protein Rca isoform ratio (Fig. 3d) did not
716 alter the temperature profile of Rubisco reactivation by Rca in the leaves of heat-treated
717 plants (Fig. 4). Interestingly, the T_{max}, T_{opt} and, to a lesser extent, $T_{0.5}$ of Rubisco reactivation
718 by Rca were higher in leaf extracts (Table 2) than the respective values measured for each
719 individual Rca isoform purified after recombinant expression (Table 1).

720

721 **Table 2. Temperature response of Rubisco activase (Rca) activity in leaf extracts.**
722 Maximum rate of Rubisco activation and corresponding temperature (T_{max}), optimum
723 temperature range (T_{opt}, above 70% activity) and temperature above the optimum at which
724 50% of the maximum activity remains ($T_{0.5}$). Values were estimated from best-fit models that
725 describe the temperature response of the pool of Rca isoforms extracted from leaves of control
726 and heat-treated cowpea on day 5 of the heatwave (Supporting Information Table S9). The
727 best-fit model for each treatment was applied to combined replicates shown in Fig. 4 (n=6-8).

Treatment	Rubisco reactivation$_{max}$ (mol $R_{A.S.}$ min^{-1})	T_{max} (°C)	T_{opt} (°C)	$T_{0.5}$ (°C)
Control	7.3	38.4	31.9 – 42.3	43.1
Heat	9.0	37.8	28.2 – 42.2	43.3

728

Discussion

Cowpea Rca isoforms differ in thermal optima

We investigated the temperature response of Rubisco activase in cowpea, a vital crop for sub-Saharan Africa that is adapted to warm temperatures, yet susceptible to the increasing pressures of global warming. Several studies in recent decades have demonstrated Rca thermolability as a limiting factor for photosynthesis at elevated temperatures (Feller *et al.*, 1998; Crafts-Brandner & Law, 2000; Salvucci *et al.*, 2006; Perdomo *et al.*, 2017). Thus, increasing Rca thermostability is a promising strategy for enhancing crop yield under elevated temperatures. We first identified four Rca isoforms in cowpea: Rca1β, Rca8α, Rca10α and Rca10β. *In vitro* characterisation of the four isoforms across a range of temperatures revealed a higher thermal optimum for Rca10α and Rca10β for both ATPase and Rubisco reactivation activities (Fig. 1b). The most abundant Rca1β and Rca8α isoforms in leaves of cowpea (Fig. 3) both exhibit lower thermal optima and thermal maxima, as well as slower rates of catalysis for both activities compared to the isoforms encoded by *Rca10* (Table 1).

Similar differences in thermal optima among isoforms have been demonstrated in other species. In rice, the α isoform is more thermotolerant however in wheat one of the two β isoforms exhibits a higher thermal optima (Scafaro *et al.*, 2018; Shivhare *et al.*, 2019; Degen *et al.*, 2020). For spinach, the β isoform demonstrates greater sensitivity to heat stress, with Rca hexamers composed solely of β isoforms displaying a lower thermal midpoint compared to homo-hexamers formed by α isoform or hetero-hexamers comprising both α and β isoforms (Keown & Pearce, 2014). Notably, for all Rca isoforms, the T_{max} for ATPase activity is higher than for Rubisco reactivation, potentially due to Rca forming higher order oligomers at elevated temperatures. Hexameric Rca is necessary for Rubisco reactivation, whilst ATP hydrolysis can occur with three Rca subunits forming an oligomer (Keown *et al.*, 2013; Hazra *et al.*, 2015). This difference potentially stems from the mechanism by which Rca reactivates Rubisco. The proposed process involves threading Rubisco through the AAA+ pore, akin to the method employed by chaperone AAA+ ATPases responsible for adjusting the conformation of misfolded proteins and facilitating reactivation (Bhat *et al.*, 2017; Houry *et al.*, 2017; Waheeda *et al.*, 2023).

The maximum rates of both Rca activities were higher for the Rca10 isoforms compared to Rca1β and Rca8α (Table 1), denoting these isoforms are faster at catalysing ATP hydrolysis and Rubisco reactivation. Similar differences among Rca isoforms were also observed in rice and wheat for ATP hydrolysis (Scafaro *et al.*, 2016; Shivhare & Mueller-Cajar, 2017; Degen *et al.*, 2020). However, the opposite was shown for Rubisco reactivation in both

764 wheat and rice with the more thermostable Rca isoforms exhibiting lower Rubisco
765 reactivation maxima compared to the less thermostable isoforms (Scafaro *et al.*, 2016,
766 2019a). This contrasts with our results and suggests that in cowpea the increased
767 thermostability of the Rca10 isoforms comes without a penalty in Rubisco reactivation rate.
768 In wheat, the thermostable TaRca1β had a higher $T_{0.5}$ than the less thermostable isoforms
769 (Scafaro *et al.*, 2019a). In cowpea, the more thermostable Rca10 isoforms have a higher $T_{0.5}$
770 than Rca1β yet comparable to Rca8α for Rubisco reactivation while $T_{0.5}$ of ATPase activity
771 was almost 10 degrees higher than in both Rca1β and Rca8α (Table 1). Furthermore,
772 Rca10α and Rca10β had a broader T_{opt} that spans and extends above the Rca1β and
773 Rca8α T_{opt} (Table 1). Similar results have been reported in wheat, where the more
774 thermotolerant TaRca1β exhibited a broader T_{opt} for ATPase activity (Degen *et al.*, 2020).
775 From these results, we postulate that Rca10α and Rca10β would be perfect candidates to
776 mediate Rubisco activity both in optimal and supra-optimal temperature conditions.
777 However, while Rca1β and Rca8α have a lower thermal tolerance, promoter analysis
778 revealed that they contain multiple stress responsive elements in their promoter region while
779 Rca10α and Rca10β have only two heat response elements (Supporting Information Fig.
780 S12) suggesting the former two isoforms may be predominantly involved in maintaining
781 Rubisco activity *in planta.*

782 Cowpea responds dynamically to a 5-day 38/28 °C heatwave

783 Cowpea plants were exposed to a five-day heatwave at the vegetative growth stage (10 °C
784 increase to 38/28 °C day/night), which is considered moderate heat stress for cowpea,
785 although this classification is dependent on the cultivar (Lonardi *et al.*, 2019; Barros *et al.*,
786 2021). Plants were well-watered to avoid confounding effects of water deficit limiting the
787 diffusion of CO_2 to Rubisco sites (Carmo-Silva *et al.*, 2012). Plant growth parameters were
788 only mildly impacted by heat, the leaf temperature only increased to 32 °C (Fig. 2) and the
789 aboveground dry biomass remained unaffected (Fig. 2c) indicating that the 5-day 38/28 °C
790 heatwave in the absence of water deficit did not constitute a severe enough heat stress to
791 impact photosynthesis and plant biomass production.

792 Other studies demonstrated that a heatwave occurring during the vegetative stage can have
793 a delayed impact on cowpea yield (Mohammed *et al.*, 2024). On day 5 of the heatwave,
794 cowpea plants showed decreased Rubisco amount, leaf thickness, total chlorophyll and TSP
795 (Fig. 2) suggesting that leaves of heat-treated plants may be experiencing accelerated leaf
796 senescence. Similar results were observed in heat-treated wheat (Qu *et al.*, 2023), and
797 could well lead to decreased biomass production should the duration of the heatwave be
798 longer. T_{crit}, an indicator of thermal lability of PSII (Perez & Feeley, 2020), corresponds to the
799 temperature at which PSII efficiency rapidly declines due to high temperature, and was

800 higher in the heat-treated plants after five days (Fig. 2). In wheat, increased T_{crit} after
801 exposure to elevated temperature in field and controlled environment experiments correlated
802 with a dynamic response of PSII to heat stress (Posch *et al.*, 2022).

803 Decreased Rubisco activity in a leaf can be due to Rubisco decarbamylation, alterations of
804 Rubisco enzymatic properties or reduced protein content (Ashton *et al.*, 2024). Rubisco
805 specific activity remained unaffected during the heatwave, indicating enzymatic properties of
806 Rubisco were not affected (Supporting Information Fig. S8). Rubisco activation state
807 decreased on day 3 of the heatwave, while on day 5 of the heatwave there was a
808 concomitant decrease in initial and total activity as well as Rubisco amount (Fig. 2d), further
809 supporting the hypothesis that heat stress caused accelerated leaf senescence.

810 Expression of thermotolerant Rca isoforms increases but remains low 811 under heat stress

812 At optimal temperatures, *Rca1β* was the most abundantly expressed, with *Rca8α* following,
813 while *Rca10α* and *Rca10β* were only marginally expressed (Fig. 3c). Under heat stress,
814 gene expression of Rca*8α*, *Rca10α* and *Rca10β* was upregulated, however expression of
815 the *Rca10* transcripts remained very low compared to *Rca1β* and *Rca8α*. The corresponding
816 protein abundance was only marginally higher for Rca8α and remained undetectable for
817 Rca10α and Rca10β (Supporting Information Fig. S13; Fig. 3d). Variation in the Rca α/β
818 ratio under optimal and supra-optimal temperatures may be attributed to differences in their
819 thermostability and regulatory mechanisms governing their activity (Zhang & Portis, 1999;
820 Wang *et al.*, 2010; Degen *et al.*, 2021). In cowpea, this ratio decreased as the leaves aged,
821 with heat-stressed plants maintaining a higher α/β ratio on day 3 of heatwave compared to
822 control pants (Fig. 3d). While Rca α is subject to redox regulation mediated by thioredoxin-f
823 (Trxf)(Zhang & Portis, 1999; Shivhare *et al.*, 2019; Kim *et al.*, 2020) and tends to be more
824 sensitive to inhibition by high ADP stromal levels (Zhang & Portis, 1999; Scafaro *et al.*,
825 2019b; Amaral *et al.*, 2024a), variation also exists in the regulatory properties of multiple Rca
826 β isoforms within a single species (Scafaro *et al.*, 2019a; Perdomo *et al.*, 2019).

827 Changes in relative abundance of Rca isoforms under heat stress are species-specific
828 (Yamori & von Caemmerer, 2009). In *Arabidopsis*, where both isoforms exhibit comparable
829 thermotolerance, heat exposure leads to an increase in both forms whilst maintaining a 1:1
830 ratio (Ristic *et al.*, 2009). Conversely, in species such as rice and wheat, where native Rca
831 isoforms differ in temperature response, heat induces upregulation of the thermotolerant
832 variants. In rice, β isoforms are predominant under optimal temperature conditions, while
833 under heat stress the more thermostable α isoform is upregulated (Scafaro *et al.*, 2018).
834 Similarly, in wheat, expression of the more thermostable TaRca1β is upregulated during

835 heat stress (Scafaro *et al.*, 2019a; Degen *et al.*, 2021). While the same was observed for
836 cowpea in the present study, the protein abundance of the thermostable Rca isoforms
837 remained below detection levels in plants exposed to the 5-day 38/28 °C heatwave. It is
838 possible that warmer or longer heatwaves might lead to significant increases in the protein
839 abundance of thermotolerant Rca isoforms. In several studies overexpression of
840 thermostable Rca via genetic engineering led to enhanced photosynthesis and yield (Kurek
841 *et al.*, 2007; Shivhare & Mueller-Cajar, 2017; Scafaro *et al.*, 2018; Degen *et al.*, 2020).
842 Increasing Rca thermostability, and to a lesser extent upregulation of its quantity, have been
843 shown to ameliorate the reduction in Rubisco activation state caused by elevated
844 temperatures (Kurek *et al.*, 2007; Scafaro *et al.*, 2018, 2019a; Kim *et al.*, 2020).

845 The temperature profile of Rubisco reactivation by Rca in cowpea leaves 846 remains unaltered under moderate heat

847 The temperature response of Rubisco reactivation in leaf extracts was determined to fully
848 understand the impact of the 5-day 38/28 °C heatwave on Rca *in planta*. Scafaro *et al.*
849 (2019a) previously reported an increase in the Rubisco reactivation rate and $T_{0.5}$ of Rca
850 extracted from leaves of heat-treated wheat. Our results showed that the Rca pool in leaf
851 extracts of heat-treated plants exhibited a similar thermal response and maintained
852 comparable thermal optima to control plants (Fig. 4). A minor, statistically insignificant
853 increase in rate was observed in cowpea while parameters T_{opt} and $T_{0.5}$ were comparable
854 between the two treatments, with a slight increase of the T_{opt} range in the heat-treated plants
855 (Table 2). The T_{opt} upper bound determined in leaf extracts was 42 °C for control and heat-
856 treated plants, much higher than the T_{leaf} in heat-treated plants (Table 2, Fig. 2a). These
857 results indicate that the heatwave in the absence of water deficit caused only mild heat
858 stress, allowing plants to respond by adjusting isoform ratios in the leaf while preserving the
859 Rca rate and temperature response.

860 Interestingly, the maximum Rca rate in leaf extracts (Table 2) was higher compared to the
861 Rubisco reactivation rate of each of the isoforms measured *in vitro* (Table 1). Similar results
862 were observed in rice and wheat but only for the more thermostable isoforms suggesting
863 differences in the heat stress response of Rca isoforms in cowpea (Scafaro *et al.*, 2016,
864 2019a). Higher Rca rate in leaf extracts may be attributed to several possible factors:
865 differences in structural conformation of recombinant Rca, post-translational modifications
866 that regulate Rca activity in the leaf and would not be present in the purified isoforms, the
867 formation of hetero-hexamers comprising different isoforms *in planta* exhibiting higher
868 thermal optima, or the interaction of Rca with other components in the chloroplast. Chen *et*
869 *al.* (2010)showed that in rice Rca can dynamically bind in a reversible way to the thylakoid

membrane while it is active and remodelling inhibited Rubisco. Binding of Rca to the thylakoid membrane has also been reported by Rokka et *al.* during heat stress although its binding to the chloroplast ribosomes was proposed to have a protective role (Rokka *et al.*, 2001, p. 20). Moreover, heat stress has been shown to induce association of Rca with β-subunit of chaperonin-60 (cpn60β), a potential heat shock molecular chaperone (Salvucci, 2008). Thus, while *in vitro* analyses are useful to compare the properties of the individual isoforms, *in vivo* analyses enable assessment of the overall Rca response within the chloroplast stroma.

Conclusion

Cowpea is a vital source of protein for sub-Saharan Africa, and depite being warm-adapted, it is threatened by future heatwaves, which are likely to increase in intensity, duration, and frequency. Here, we identified two isoforms of Rca that have higher thermal maxima, broader thermal optima, and faster rates of ATP hydrolysis and Rubisco reactivation than the predominant Rca isoforms present in cowpea leaves. We showed that a 5-day 38/28 °C heatwave in the absence of water deficit caused leaf temperature to increase to 32 °C. Since this temperature is below the temperature at which Rca activity for each Rca isoform decreased below 70% of maximum, the impact of such a heatwave on Rubisco function and biomass production was only mild. However, cowpea plants growing in smallholder farmer fields in sub-Saharan Africa are likely to experience water deficit alongside warmer heatwaves (Almazroui *et al.*, 2020; Song *et al.*, 2023). This combination can impact the ability of the plant to cool its leaves leading to higher leaf temperatures (Carmo-Silva *et al.*, 2012; Fahad *et al.*, 2017; Sato *et al.*, 2024). Increasing the abundance of the superior Rca10α and Rca10β isoforms characterised here provides an exciting opportunity to enhance the resilience of cowpea and other crops to future extreme climates.

Acknowledgements:
We thank Dr Sam Taylor (Lancaster University) for input and discussions around experimental design and calculations for determining T_{crit}. Ben Davies (Lancaster University) supported plant maintenance, measurements and sampling. We thank Dr Rachel Baxter (Lancaster University) for assistance with data analysis, and Dr Joana Amaral for useful discussions on data interpretation.

Competing interests:
The authors declare no conflicts of interest.

Author contributions:
E.C.S conceived and supervised the research. A.G., R.P., I.R., D.J.O., E.C.S. designed experiments. M.T.P. designed and executed the cloning strategy. D.B., P.D.G., D.W. produced and purified recombinant proteins. D.W. and C.J.A. purified Rubisco. D.B. and A.G. performed ATP hydrolysis measurements. A.G. performed Rubisco reactivation measurements. R.P. and I.R. performed heatwave experiments. R.P. performed RNAseq, RT-qPCR and plant growth measurements. R.P. and P.D.G. performed promoter analyses. I.R. performed fluorescence measurements. A.G., R.P. and C.J.A. determined activity and amount of Rubisco and Rubisco activase in leaf extracts. A.G., R.P., C.J.A. and I.R. analysed the data. A.G. and E.C.S. wrote the manuscript with help from all authors.

Data availability:
Data presented are available in the accompanying supporting information and source data. The RNA-seq data reported in this article has been deposited in DDBJ's Sequence Read Archive (DRA) and are accessible through DRR BioProject accession number PRJDB19806. Processed RNA-seq data are submitted in the DDBJ's Genomic Expression Archive (GEA) and are accessible through the Experiment accession number (E-GEAD-889). Other data associated with the study are available from the corresponding author.

Funding:
This work was supported by the project Realizing Increased Photosynthetic Efficiency (RIPE), that is funded by Gates Agricultural Innovations grant investment 57248, awarded to Lancaster University by the University of Illinois, USA. D.B. was supported by a PhD scholarship from Lancaster University.

928 # References

929 **Akaike H**. **1974**. A new look at the statistical model identification. *IEEE Transactions on*
930 *Automatic Control* **19**: 716–723.

931 **Almazroui M, Saeed F, Saeed S, Nazrul Islam M, Ismail M, Klutse NAB, Siddiqui MH**.
932 **2020**. Projected change in temperature and precipitation over Africa from CMIP6. *Earth*
933 *Systems and Environment* **4**: 455–475.

934 **Amaral J, Lobo AKM, Carmo-Silva E**. **2024a**. Regulation of Rubisco activity in crops. *New*
935 *Phytologist* **241**: 35–51.

936 **Amaral J, Lobo AKM, Carmo-Silva E, Orr DJ**. **2024b**. Purification of Rubisco from Leaves.
937 In: Covshoff S, ed. Photosynthesis : Methods and Protocols. New York, NY: Springer US, 417–
938 426.

939 **Ara N, Nakkanong K, Lv W, Yang J, Hu Z, Zhang M**. **2013**. Antioxidant enzymatic activities
940 and gene expression associated with heat tolerance in the stems and roots of two Cucurbit
941 species ('*Cucurbita maxima*' and '*Cucurbita moschata*') and their interspecific inbred line
942 "*Maxchata*". *International Journal of Molecular Sciences* **14**: 24008.

943 **Ashton CJ, Page R, Lobo AKM, Amaral J, Siqueira JA, Orr DJ, Carmo-Silva E**. **2024**.
944 Radiometric determination of Rubisco activation state and quantity in leaves. In: Methods in
945 Enzymology. Academic Press.

946 **Bagati S, Rai GK, Bhadwal D, Berwal MK**. **2021**. Biotechnological approaches for the
947 development of heat stress tolerance in crop plants. In: Abiotic Stress Tolerance Mechanisms
948 in Plants. CRC Press.

949 **Barros JRA, Guimarães MJM, Silva RM e, Rêgo MTC, de Melo NF, de Melo Chaves AR,**
950 **Angelotti F**. **2021**. Selection of cowpea cultivars for high temperature tolerance: physiological,
951 biochemical and yield aspects. *Physiology and Molecular Biology of Plants* **27**: 29–38.

952 **Barta C, Carmo-Silva AE, Salvucci ME**. **2011**. Purification of Rubisco activase from leaves
953 or after expression in *Escherichia coli*. *Methods in Molecular Biology (Clifton, N.J.)* **684**: 363–
954 374.

955 **Becker R, Schüth C, Merz R, Khaliq T, Usman M, Beek T aus der, Kumar R, Schulz S**.
956 **2023**. Increased heat stress reduces future yields of three major crops in Pakistan's Punjab
957 region despite intensification of irrigation. *Agricultural Water Management* **281**: 108243.

958 **Bhat JY, Thieulin-Pardo G, Hartl FU, Wendler P, Mili Ci C G, Bracher A, Maxwell A,**
959 **Ciniawsky S, Mueller-Cajar O, Engen JR, *et al.* 2017**. Mechanism of enzyme repair by the
960 AAA + chaperone Rubisco activase. *Molecular Cell* **67**: 744–756.

961 **Blighe, K, S Rana, M Lewis**. **2018**. EnhancedVolcano: Publication-ready volcano plots with
962 enhanced colouring and labeling.

963 **Bloemers D, Carmo-Silva E**. **2024**. Antibody design for the quantification of photosynthetic
964 proteins and their isoforms. In: Covshoff S, ed. Photosynthesis : Methods and Protocols. New
965 York, NY: Springer US, 405–416.

966 **Bradford MM**. **1976**. A rapid and sensitive method for the quantitation of microgram quantities
967 of protein utilizing the principle of protein-dye binding. *Analytical Biochemistry* **72**: 248–254.

968 **Bretz F, Hothorn T, Westfall P**. **2016**. *Multiple Comparisons Using R*. CRC Press.

969 **Brown AV, Conners SI, Huang W, Wilkey AP, Grant D, Weeks NT, Cannon SB, Graham**
970 **MA, Nelson RT**. **2021**. A new decade and new data at SoyBase, the USDA-ARS soybean
971 genetics and genomics database. *Nucleic Acids Research* **49**: D1496–D1501.

972 **Carmo-Silva AE, Gore MA, Andrade-Sanchez P, French AN, Hunsaker DJ, Salvucci ME**.
973 **2012**. Decreased CO_2 availability and inactivation of Rubisco limit photosynthesis in cotton
974 plants under heat and drought stress in the field. *Environmental and Experimental Botany* **83**:
975 1–11.

976 **Carmo-Silva AE, Salvucci ME**. **2011**. The activity of Rubisco's molecular chaperone,
977 Rubisco activase, in leaf extracts. *Photosynthesis Research* **108**: 143–155.

978 **Carmo-Silva AE, Salvucci ME**. **2013**. The Regulatory Properties of Rubisco Activase Differ
979 among Species and Affect Photosynthetic Induction during Light Transitions 1. *Plant*
980 *Physiology Ȯ* **161**: 1645–1655.

981 **Carmo-Silva E, Scales JC, Madgwick PJ, Parry MAJ**. **2015**. Optimizing Rubisco and its
982 regulation for greater resource use efficiency. *Plant, Cell & Environment* **38**: 1817–1832.

983 **Chen H**. **2022**. VennDiagram: Generate High-Resolution Venn and Euler Plots.

984 **Chen J-H, Tang M, Jin X-Q, Li H, Chen L-S, Wang Q-L, Sun A-Z, Yi Y, Guo F-Q**. **2022**.
985 Regulation of Calvin–Benson cycle enzymes under high temperature stress. *aBIOTECH* **3**:
986 65.

987 **Chen J, Wang P, Mi H-L, Chen G-Y, Xu D-Q**. **2010**. Reversible association of ribulose-1, 5-
988 bisphosphate carboxylase/oxygenase activase with the thylakoid membrane depends upon
989 the ATP level and pH in rice without heat stress. *Journal of Experimental Botany* **61**: 2939–
990 2950.

991 **Chifflet S, Torriglia A, Chiesa R, Tolosa S**. **1988**. A method for the determination of inorganic
992 phosphate in the presence of labile organic phosphate and high concentrations of protein:
993 Application to lens ATPases. *Analytical Biochemistry* **168**: 1–4.

994 **Crafts-Brandner SJ, Law RD**. **2000**. Effect of heat stress on the inhibition and recovery of
995 the ribulose-1,5-bisphosphate carboxylase/oxygenase activation state. *Planta* **212**: 67–74.

996 **Crafts-Brandner SJ, Salvucci ME**. **2000**. Rubisco activase constrains the photosynthetic
997 potential of leaves at high temperature and CO_2. *Proceedings of the National Academy of*
998 *Sciences of the United States of America* **97**: 13430–13435.

999 **Degen GE, Orr DJ, Carmo-Silva E**. **2021**. Heat-induced changes in the abundance of wheat
1000 Rubisco activase isoforms. *New Phytologist* **229**: 1298–1311.

1001 **Degen GE, Worrall D, Carmo-Silva E**. **2020**. An isoleucine residue acts as a thermal and
1002 regulatory switch in wheat Rubisco activase. *Plant Journal* **103**: 742–751.

1003 **Fahad S, Bajwa AA, Nazir U, Anjum SA, Farooq A, Zohaib A, Sadia S, Nasim W, Adkins**
1004 **S, Saud S, *et al.* 2017**. Crop production under drought and heat stress: Plant responses and
1005 management options. *Frontiers in Plant Science* **8**.

1006 **Feller U, Crafts-Brandner SJ, Salvucci ME**. **1998**. Moderately high temperatures inhibit
1007 ribulose-1,5-bisphosphate carboxylase/oxygenase (Rubisco) activase-mediated activation of
1008 Rubisco. *Plant Physiol* **116**: 539–546.

1009 **Galmés J, Hermida-Carrera C, Laanisto L, Niinemets Ü**. **2016**. A compendium of
1010 temperature responses of Rubisco kinetic traits: variability among and within photosynthetic
1011 groups and impacts on photosynthesis modeling. *Journal of Experimental Botany* **67**: 5067–
1012 5091.

1013 **Gonçalves A, Goufo P, Barros A, Domínguez-Perles R, Trindade H, Rosa EAS, Ferreira**
1014 **L, Rodrigues M**. **2016**. Cowpea (*Vigna unguiculata* L. Walp), a renewed multipurpose crop
1015 for a more sustainable agri-food system: nutritional advantages and constraints. *Journal of the*
1016 *Science of Food and Agriculture* **96**: 2941–2951.

1017 **Goodstein DM, Shu S, Howson R, Neupane R, Hayes RD, Fazo J, Mitros T, Dirks W,**
1018 **Hellsten U, Putnam N, *et al.* 2012**. Phytozome: a comparative platform for green plant
1019 genomics. *Nucleic Acids Research* **40**: D1178–D1186.

1020 **Graves S, Piepho H-P, Selzer L, Dorai-Raj S**. **2024**. multcompView: Visualizations of Paired
1021 Comparisons.

1022 **Harboure P**. **2024**. WMO Global Annual to Decadal Climate Update.

1023 **Hatfield JL, Prueger JH**. **2011**. Agroecology: Implications for Plant Response to Climate
1024 Change. In: Crop Adaptation to Climate Change. Wiley-Blackwell.

1025 **Hazra S, Henderson JN, Liles K, Hilton MT, Wachter RM**. **2015**. Regulation of ribulose-1,5-
1026 bisphosphate carboxylase/oxygenase (Rubisco) activase. *The Journal of Biological Chemistry*
1027 **290**: 24222–24236.

1028 **Hermida-Carrera C, Kapralov MV, Galmés J**. **2016**. Rubisco catalytic properties and
1029 temperature response in crops. *Plant Physiology* **171**: 2549.

1030 **Houry WA, Wachter R, Prahlad V, Hayer-Hartl M, Bhat JY, Thieulin-Pardo G, Hartl FU**.
1031 **2017**. Rubisco activases: AAA+ chaperones adapted to enzyme repair. *Frontiers in Molecular*
1032 *Biosciences* **4**: 20.

1033 **Kassambara A**. **2023**. ggpubr: 'ggplot2' Based Publication Ready Plots.

1034 **Keown JR, Griffin MDW, Mertens HDT, Pearce FG**. **2013**. Small oligomers of ribulose-
1035 bisphosphate carboxylase/oxygenase (Rubisco) activase are required for biological activity.
1036 *The Journal of Biological Chemistry* **288**: 20607–20615.

1037 **Keown JR, Pearce FG**. **2014**. Characterization of spinach ribulose-1,5-bisphosphate
1038 carboxylase/ oxygenase activase isoforms reveals hexameric assemblies with increased
1039 thermal stability. *Biochem. J* **464**: 413–423.

1040 **Kilian J, Whitehead D, Horak J, Wanke D, Weinl S, Batistic O, D'Angelo C, Bornberg-**
1041 **Bauer E, Kudla J, Harter K**. **2007**. The AtGenExpress global stress expression data set:
1042 protocols, evaluation and model data analysis of UV-B light, drought and cold stress
1043 responses. *The Plant Journal* **50**: 347–363.

1044 **Kim SY, Stessman DJ, Wright DA, Spalding MH, Huber SC, Ort DR**. **2020**. *Arabidopsis*
1045 plants expressing only the redox-regulated Rca-α isoform have constrained photosynthesis
1046 and plant growth. *Plant Journal* **103**: 2250–2262.

1047 **Kumar A, Li C, Portis AR**. **2009**. *Arabidopsis thaliana* expressing a thermostable chimeric
1048 Rubisco activase exhibits enhanced growth and higher rates of photosynthesis at moderately
1049 high temperatures. *Photosynthesis Research* **100**: 143–153.

1050 **Kurek I, Chang TK, Bertain SM, Madrigal A, Liu L, Lassner MW, Zhu G**. **2007**. Enhanced
1051 thermostability of *Arabidopsis* Rubisco activase improves photosynthesis and growth rates
1052 under moderate heat stress. *The Plant Cell* **19**: 3230–3241.

1053 **Law RD, Crafts-Brandner SJ**. **2001**. High temperature stress increases the expression of
1054 wheat leaf ribulose-1,5-bisphosphate carboxylase/oxygenase activase protein. *Archives of*
1055 *Biochemistry and Biophysics* **386**: 261–267.

1056 **Li G, Mao H, Ruan X, Xu Q, Gong Y, Zhang X, Zhao N**. **2002**. Association of heat-induced
1057 conformational change with activity loss of Rubisco. *Biochemical and Biophysical Research*
1058 *Communications* **290**: 1128–1132.

1059 **Liang Q, Muñoz-Amatriaín M, Shu S, Lo S, Wu X, Carlson JW, Davidson P, Goodstein**
1060 **DM, Phillips J, Janis NM, *et al.* 2024**. A view of the pan-genome of domesticated cowpea
1061 (*Vigna unguiculata* [L.] Walp.). *The Plant Genome* **17**: e20319.

1062 **Lichtenthaler HK**. **1987**. [34] Chlorophylls and carotenoids: Pigments of photosynthetic
1063 biomembranes. In: Plant Cell Membranes. Methods in Enzymology. Academic Press, 350–
1064 382.

1065 **Lin Pedersen T**. **2024**. patchwork: The Composer of Plots.

1066 **Lonardi S, la Mu~ Noz-Amatria In M, Liang Q, Shu S, Wanamaker SI, Lo S, Tanskanen**
1067 **J, Schulman AH, Zhu T, Luo M-C, *et al.* 2019**. The genome of cowpea (*Vigna unguiculata*
1068 [L.] Walp.). *The Plant Journal* **98**: 767–782.

1069 **Martin M**. **2011**. Cutadapt removes adapter sequences from high-throughput sequencing
1070 reads. *EMBnet.journal* **17**: 10.

1071 **Mathur S, Agrawal D, Jajoo A**. **2014**. Photosynthesis: Response to high temperature stress.
1072 *Journal of Photochemistry and Photobiology B: Biology* **137**: 116–126.

1073 **Mohammed SB, Ongom PO, Togola A, Boukar O**. **2024**. Enhancing Cowpea tolerance to
1074 elevated temperature: Achievements, challenges and future directions. *Agronomy* **14**: 513.

1075 **Moore CE, Meacham-Hensold K, Lemonnier P, Slattery RA, Benjamin C, Bernacchi CJ,**
1076 **Lawson T, Cavanagh AP**. **2021**. The effect of increasing temperature on crop photosynthesis:
1077 from enzymes to ecosystems. *Journal of Experimental Botany* **72**: 2822–2844.

1078 **Muggeo VMR**. **2017**. Interval estimation for the breakpoint in segmented regression: a
1079 smoothed score-based approach. *Australian & New Zealand Journal of Statistics* **59**: 311–
1080 322.

1081 **Murchie EH, Lawson T**. **2013**. Chlorophyll fluorescence analysis: a guide to good practice
1082 and understanding some new applications. *Journal of Experimental Botany* **64**: 3983–3998.

1083 **Nagarajan R, Gill KS**. **2018**. Evolution of Rubisco activase gene in plants. *Plant Molecular*
1084 *Biology* **96**: 69–87.

1085 **Orr DJ, Robijns AKJ, Baker CR, Niyogi KK, Carmo-Silva E**. **2023**. Dynamics of Rubisco
1086 regulation by sugar phosphate derivatives and their phosphatases. *Journal of Experimental*
1087 *Botany* **74**: 581–590.

1088 **Patro R, Duggal G, Love MI, Irizarry RA, Kingsford C**. **2017**. Salmon provides fast and bias-
1089 aware quantification of transcript expression. *Nature Methods* **14**: 417–419.

1090 **Perdomo JA, Buchner P, Carmo-Silva E**. **2021**. The relative abundance of wheat Rubisco
1091 activase isoforms is post-transcriptionally regulated. *Photosynthesis Research* **148**: 47–56.

1092 **Perdomo JA, Capó-Bauçà S, Carmo-Silva E, Galmés J**. **2017**. Rubisco and Rubisco
1093 activase play an important role in the biochemical limitations of photosynthesis in rice, wheat,
1094 and maize under high temperature and water deficit. *Frontiers in Plant Science* **8**: 490.

1095 **Perdomo JA, Degen GE, Worrall D, Carmo-Silva E**. **2019**. Rubisco activation by wheat
1096 Rubisco activase isoform 2β is insensitive to inhibition by ADP. *Biochemical Journal* **476**:
1097 2595–2606.

1098 **Perdomo JA, Sales CRG, Carmo-Silva E**. **2018**. Quantification of photosynthetic enzymes
1099 in leaf extracts by immunoblotting. *Methods in Molecular Biology (Clifton, N.J.)* **1770**: 215–
1100 227.

1101 **Perez TM, Feeley KJ**. **2020**. Photosynthetic heat tolerances and extreme leaf temperatures.
1102 *Functional Ecology* **34**: 2236–2245.

1103 **Portis AR**. **2003**. Rubisco activase - Rubisco's catalytic chaperone. *Photosynthesis Research*
1104 **75**: 11–27.

1105 **Portis AR, Li C, Wang D, Salvucci ME**. **2008**. Regulation of Rubisco activase and its
1106 interaction with Rubisco. *Journal of Experimental Botany* **59**: 1597–1604.

1107 **Posch BC, Hammer J, Atkin OK, Bramley H, Ruan Y-L, Trethowan R, Coast O**. **2022**.
1108 Wheat photosystem II heat tolerance responds dynamically to short- and long-term warming.
1109 *Journal of Experimental Botany* **73**: 3268–3282.

1110 **Qu L, Gu X, Li J, Guo J, Lu D**. **2023**. Leaf photosynthetic characteristics of waxy maize in
1111 response to different degrees of heat stress during grain filling. *BMC Plant Biology* **23**: 469.

1112 **Ristic Z, Momčilović I, Bukovnik U, Prasad PVV, Fu J, DeRidder BP, Elthon TE,**
1113 **Mladenov N**. **2009**. Rubisco activase and wheat productivity under heat-stress conditions.
1114 *Journal of Experimental Botany* **60**: 4003–4014.

1115 **Robinson SP, Portis AR**. **1989**. Adenosine triphosphate hydrolysis by purified Rubisco
1116 activase. *Archives of Biochemistry and Biophysics* **268**: 93–99.

1117 **Rokka A, Zhang L, Aro EM**. **2001**. Rubisco activase: An enzyme with a temperature-
1118 dependent dual function? *Plant Journal* **25**: 463–471.

1119 **Ruuska S, Andrews TJ, Badger MR, Hudson GS, Laisk A, Price GD, Caemmerer S von**.
1120 **1998**. The interplay between limiting processes in C3 photosynthesis studied by rapid-
1121 response gas exchange using transgenic tobacco impaired in photosynthesis. *Functional*
1122 *Plant Biology* **25**: 859–870.

Sales CRG, Molero G, Evans JR, Taylor SH, Joynson R, Furbank RT, Hall A, Carmo-Silva E. **2022**. Phenotypic variation in photosynthetic traits in wheat grown under field versus glasshouse conditions. *Journal of Experimental Botany* **73**: 3221–3237.

Salvucci ME. **2008**. Association of Rubisco activase with chaperonin-60b: a possible mechanism for protecting photosynthesis during heat stress. *Journal of Experimental Botany* **59**: 1923–1933.

Salvucci ME, Crafts-Brandner SJ. **2004**. Relationship between the heat tolerance of photosynthesis and the thermal stability of Rubisco activase in plants from contrasting thermal environments. **134**: 1460–1470.

Salvucci ME, DeRidder BP, Portis AR. **2006**. Effect of activase level and isoform on the thermotolerance of photosynthesis in Arabidopsis. *Journal of Experimental Botany* **57**: 3793–3799.

Salvucci ME, Osteryoung KW, Crafts-Brandner SJ, Vierling E. **2001**. Exceptional Sensitivity of Rubisco Activase to Thermal Denaturation in Vitro and in Vivo. *Plant Physiology* **127**: 1053–1064.

Sato H, Mizoi J, Shinozaki K, Yamaguchi-Shinozaki K. **2024**. Complex plant responses to drought and heat stress under climate change. *The Plant Journal* **117**: 1873–1892.

Scafaro AP, Atwell BJ, Muylaert S, Reusel BV, Ruiz GA, Rie JV, Gallé A. **2018**. A thermotolerant variant of Rubisco activase from a wild relative improves growth and seed yield in rice under heat stress. *Frontiers in Plant Science* **9**: 1663.

Scafaro AP, Bautsoens N, den Boer B, Van Rie J, Gallé A. **2019a**. A Conserved sequence from heat-adapted species improves Rubisco activase thermostability in wheat. *Plant Physiology* **181**: 43–54.

Scafaro AP, Gallé A, Van Rie J, Carmo-Silva E, Salvucci ME, Atwell BJ. **2016**. Heat tolerance in a wild *Oryza* species is attributed to maintenance of Rubisco activation by a thermally stable Rubisco activase ortholog. *New Phytologist* **211**: 899–911.

Scafaro AP, Posch BC, Evans JR, Farquhar GD, Atkin OK. **2023**. Rubisco deactivation and chloroplast electron transport rates co-limit photosynthesis above optimal leaf temperature in terrestrial plants. *Nature Communications* **14**: 2820.

Scafaro AP, Vleesschauwer DD, Bautsoens N, Hannah MA, Boer B den, Gallé A, Rie JV. **2019b**. A single point mutation in the C-terminal extension of wheat Rubisco activase dramatically reduces ADP inhibition via enhanced ATP binding affinity. *The Journal of Biological Chemistry* **294**: 17931.

Serban AJ, Breen IL, Bui HQ, Levitus M, Rebekka Wachter XM, Jez JM. **2018**. Assembly–disassembly is coupled to the ATPase cycle of tobacco Rubisco activase. *J. Biol. Chem* **293**: 19451–19465.

Shivhare D, Mueller-Cajar O. **2017**. *In vitro* characterization of thermostable CAM Rubisco activase reveals a Rubisco interacting surface loop. **174**: 1505–1516.

Shivhare D, Ng J, Tsai Y-CC, Mueller-Cajar O. **2019**. Probing the rice Rubisco-Rubisco activase interaction via subunit heterooligomerization. *Proceedings of the National Academy of Sciences of the United States of America* **116**: 24041–24048.

Song J, Tong G, Chao J, Chung J, Zhang M, Lin W, Zhang T, Bentler PM, Zhu W. **2023**. Data driven pathway analysis and forecast of global warming and sea level rise. *Scientific Reports* **13**: 5536.

Song K, Yim WC, Lee B-M. **2017**. Expression of heat shock proteins by heat stress in soybean. *Plant Breeding and Biotechnology* **5**: 344–353.

Stainbrook SC, Aubuchon LN, Chen A, Johnson E, Si A, Walton L, Ahrendt AJ, Strenkert D, Jez JM. **2024**. C4 grasses employ distinct strategies to acclimate Rubisco activase to heat stress. *Bioscience Reports* **44**.

Stotz M, Mueller-Cajar O, Ciniawsky S, Wendler P, Hartl FU, Bracher A, Hayer-Hartl M. **2011**. Structure of green-type Rubisco activase from tobacco. *Nature Structural & Molecular Biology* **18**: 1366–1370.

Taylor SH, Gonzalez-Escobar E, Page R, Parry MAJ, Long SP, Carmo-Silva E. **2022**. Faster than expected Rubisco deactivation in shade reduces cowpea photosynthetic potential in variable light conditions. *Nature Plants* **8**: 118–124.

Taylor SH, Orr DJ, Carmo-Silva E, Long SP. **2020**. During photosynthetic induction, biochemical and stomatal limitations differ between Brassica crops. *Plant, Cell & Environment* **43**: 2623–2636.

Waheeda K, Kitchel H, Wang Q, Chiu P-L. **2023**. Molecular mechanism of Rubisco activase: Dynamic assembly and Rubisco remodeling. *Frontiers in Molecular Biosciences* **10**: 1125922.

Wang D, Li X-F, Zhou Z-J, Feng X-P, Yang W-J, Jiang D-A. **2010**. Two Rubisco activase isoforms may play different roles in photosynthetic heat acclimation in the rice plant. *Physiologia Plantarum* **139**: 55–67.

Warrag MOA, Hall AE. **1984**. Reproductive responses of cowpea (*Vigna unguiculata* (L.) Walp.) to heat stress. II. Responses to night air temperature. *Field Crops Research* **8**: 17–33.

Weber E, Engler C, Gruetzner R, Werner S, Marillonnet S. **2011**. A modular cloning system for standardized assembly of multigene constructs. *PLOS ONE* **6**: e16765.

Werner S, Engler C, Weber E, Gruetzner R, Marillonnet S. **2012**. Fast track assembly of multigene constructs using Golden Gate cloning and the MoClo system. *Bioengineered Bugs* **3**: 38–43.

Wickham H. **2017**. Tidyverse: Easily install and load the 'tidyverse'. *R package version* **1**: 2017.

Wijewardene I, Shen G, Zhang H. **2021**. Enhancing crop yield by using Rubisco activase to improve photosynthesis under elevated temperatures. **1**: 2.

Winter D, Vinegar B, Nahal H, Ammar R, Wilson GV, Provart NJ. **2007**. An "Electronic fluorescent pictograph" browser for exploring and analyzing large-scale biological data sets. *PLOS ONE* **2**: e718.

Wood SN. **2017**. *Generalized Additive Models: An Introduction with R, Second Edition*. New York: Chapman and Hall/CRC.

Yamori W, von Caemmerer S. **2009**. Effect of Rubisco activase deficiency on the temperature response of CO_2 assimilation rate and Rubisco activation state: Insights from

transgenic tobacco with reduced amounts of Rubisco activase. *Plant Physiology* **151**: 2073–2082.

Yin Z, Zhang Z, Deng D, Chao M, Gao Q, Wang Y, Yang Z, Bian Y, Hao D, Xu C. **2014**. Characterization of Rubisco activase genes in maize: An α-isoform gene functions alongside a β-isoform gene. *Plant Physiology* **164**: 2096–2106.

Zahra N, Hafeez MB, Wahid A, Al Masruri MH, Ullah A, Siddique KHM, Farooq M. **2023**. Impact of climate change on wheat grain composition and quality. *Journal of the Science of Food and Agriculture* **103**: 2745–2751.

Zhang N, Kallis RP, Ewy RG, Portis AR. **2002**. Light modulation of Rubisco in *Arabidopsis* requires a capacity for redox regulation of the larger Rubisco activase isoform. *Proceedings of the National Academy of Sciences of the United States of America* **99**: 3330–3334.

Zhang N, Portis AR. **1999**. Mechanism of light regulation of Rubisco: A specific role for the larger Rubisco activase isoform involving reductive activation by thioredoxin-f. *Plant Biology* **96**: 9438–9443.

1219 # Supporting Information

1220 **Supporting Information Figures**

1221 Fig. S1. Amino acid residue alignment of the four cowpea Rca isoforms.

1222 Fig. S2. *In vitro* Rubisco reactivation by the four cowpea Rca isoforms.

1223 Fig. S3. Heatwave experimental design and cabinet temperature monitoring.

1224 Fig. S4. Cabinet plant layout design.

1225 Fig. S5. Leaf temperature monitoring over the heatwave experiment.

1226 Fig. S6. Growth parameters and chlorophyll content during and after heat stress.

1227 Fig. S7. T_{crit} calculation from temperature response of chlorophyll fluorescence-derived Fv/Fm.

1228 Fig. S8. Specific Rubisco activities of control and heat-treated plants.

1229 Fig. S9. Differential gene expression in heat-treated *versus* control cowpea plants.

1230 Fig. S10. Volcano plots depicting differential gene expression based on log change across the
1231 days of heatwave.

1232 Fig. S11. Gene expression of heat shock protein 20 (HSP20) and cowpea Rca transcripts.

1233 Fig. S12. Potential cis-acting regulatory elements in cowpea Rca promoter regions.

1234 Fig. S13. Protein abundance of Rca isoforms in leaves of control and heat-treated plants.

1235 Fig. S14. Protocol outline for determination of Rca activity in leaf extracts (LE).

1236 Fig. S15. Rubisco reactivation by the pool of cowpea Rca isoforms in leaf extracts (LE).

1237 **Supporting Information Tables**

1238 Table S1. Reference protein sequences used to identify cowpea Rca genes.

1239 Table S2. Primer sequences for adding Golden Gate overhangs to Rca coding regions.

1240 Table S3. Optimum temperature of in vitro Rubisco activase (Rca) activity.

1241 Table S4. Modelling of the *in vitro* temperature response of ATP hydrolysis and Rubisco
1242 activation by cowpea Rca isoforms.

1243 Table S5. RNA sample QC analysis prior to RNA sequencing.

1244 Table S6. Sequencing and alignment statistics.

1245 Table S7. MIQE checklist for RT-qPCR.

1246 Table S8. RT-qPCR primers.

1247 Table S9. Modelling of the temperature response of Rubisco activation by cowpea Rca in leaf
1248 extracts of control and heat-treat plants.

1249 Table S10. Leaf total soluble protein (TSP) and chlorophyll content.

1250 References